MODELING OF THE INTERACTION BETWEEN COLON AND COLONOSCOPE DURING A COLONOSCOPY

A DISSERTATION
SUBMITTED TO THE FACULTY OF THE GRADUATE SCHOOL OF THE
UNIVERSITY OF MINNESOTA
BY

Xuehuan He

IN PARTIAL FULFILLMENT OF THE REQUIREMENT FOR
DEGREE OF MASTER OF SCIENCE

Adviser: Dr. Debao Zhou

May 2018

© Copyright by Xuehuan He. 2018

All Rights Reserved

ACKNOWLEDGEMENTS

I would like to extend my sincere gratitude to everyone involved in making this report possible. I owe my special thanks to Dr. Debao Zhou, who is the supervisor of my master's degree in UMD, for his support, instructions, and encouragement over the past two years.

Furthermore, I would like to thank Zahra Sadat Navabi Ghamsari, for helping me finding the porcine colon and designing the experiment set-up, and Mathew Orner, for assisting me using the tensile test machine.

Thanks to my thesis committee members, Dr. Ping Zhao and Dr. Jing Bai, and finally, to my parents for their unwavering support, great trusts and encouragements. I am also so grateful to all the faculties and staffs who once taught in classes and whom I once worked with and my fellow graduate students. They made my life in UMD most wonderful.

DEDICATION

This dissertation is dedicated to my parents.

For your everlasting love.

ABSTRACT

One of the main complications in completing a colonoscopy is that the colonoscope causes patient pain during the procedure. To reduce patient pain, small-caliber (SC) colonoscopes have been developed. To evaluate the efficacy of SC colonoscopes in reducing patient pain with that of traditional standard colonoscope (SDC), several randomized control trials (RCTs) were conducted and showed varying results, with some showed benefits whereas others did not. Among these RCTs, patient characteristics, including gender, age, and region were varied and further assumed to be responsible for the varied results. However, the influence of patient characteristics on the efficacy of SC colonoscopes in terms of reducing patient pain is still unclear due to many unavoidable disturbing factors in RCTs, including endoscopists' skills, bowel preparation methods, and other new beneficial features of colonoscopes (passive bending and high force transmission shaft). Therefore, to explore the influence of gender, age, and region of patients on the efficacy of SC colonoscopes in terms of reducing patient pain, a numerical model could overcome the limitations of RCTs and provide such insight is developed in our work.

As a first step, the structural differences of the human colon with respect to gender, age, and region were analyzed and summarized, which further functions as the basis of the development of colon models and their boundary conditions. As a result, three normalized colon segments were selected and modelled, including rectosigmoid

junction (RCJ), rectum-splenic flexure (RSF), and transverse-hepatic flexure (THF) models. The colonoscope was modelled as a thin and flexible cylinder with a hemisphere tip. Three different diameters were applied to colonoscope models, including 9.2mm for ultrathin colonoscope (UTC), 11.3mm for pediatric colonoscope (PDC), and 12.8mm for standard colonoscope (SDC). UTC and PDC were classified as SC colonoscopes.

In the stage of insertion simulation, a comparison between implicit and explicit finite element solution method was conducted, and then an explicit solver ANSYS-LSDYNA was selected to simulate the insertion process of colonoscopes in colon models. An uni-axial tension test was carried out to provide the experimental data of a porcine colon, and then an optimization procedure with the use of ANSYS and Optislang programs was performed to provide the necessary parameters of the constitutive material model of the colonic tissue. By comparing colon deformation during the insertion simulation, patient pain induced by colonoscopes were further predicted.

The model developed in this research serves as a starting point in understanding the efficacy of SC colonoscopes in reducing patient pain considering the effects of patient characteristics, including gender, age, and region. This model may also provide scientific guidelines for the selection of patient specified colonoscope

Table of Contents

ACKNOWLEDGEMENTS i

DEDICATION ii

ABSTRACT iii

List of Figures vii

List of Tables x

CHAPTER I 1

INTRODUCTION 1

1.1 Research Background 1

1.1.1 Anatomy and Constraints of Colon 1

1.1.2 Colonoscopy Procedure and Patient Pain 2

1.1.3 Technical Affecting Factors on Patient Pain 2

1.1.4 Randomized Controlled Trials 6

1.2 Research Motivation 8

1.3 Scope 8

CHAPTER II 10

REVIEW OF LITERATURE 10

2.1 Previous Work 10

2.2 Anatomic Characteristics of Human Colons 11

2.3 Finite Element Solution Method 12

2.3.1. Introduction to Implicit Finite Element Solution Method 13

2.3.2. Introduction to Explicit Finite Element Solution Method 18

2.3.3. Selection of Finite Element Solution Method 20

2.4 Constitutive Modelling of Colon Tissue 21

CHAPTER III 25

INSERTION SIMULATION 25

3.1 Geometry and Mesh 25

3.2 Material Properties 28

3.3 Boundary Conditions 29

3.4 Quasi-Static Modelling 31

CHAPTER IV 37

MATERIAL PARAMETERS OPTIMIZATION 37
4.1 Introduction 37
4.2 Experimental and Numerical Analysis 38
4.2.1 Experimental Details 38
4.2.2 Computational Model 39
4.2.3 Optimization Objective Function 40
4.3 Optimization Procedures and Results 41
CHAPTER V 46
SIMULATION RESULTS 46
5.1 Influence of Age 46
5.2 Influence of region 50
5.3 Influence of Gender 53
5.3.1 Simulation results of RSF model 53
5.3.2 Simulation results of THF model 57
5.4 Simulation results of fixed THF model 61
CHAPTER VI 68
CONCLUSIONS AND FUTURE WORK 68
6.1 Conclusions 68
6.2 Future Work 70
REFERENCE 72

List of Figures

Fig. 1- 1 Human colon anatomy 1

Fig. 1- 2 Three stages of colonoscope advancement through the angulation of the sigmoid colon..... 4

Fig. 1- 3 Sigmoid colon deformation induced by the scope shaft 5

Fig. 1- 4 The structure of colonoscope insertion tube 5

Fig. 3- 1 Spline used for Rectosigmoid Junction Model (RSJ) 26

Fig. 3- 2 Spline used for Rectum-Splenic Flexure Model(RSF) 27

Fig. 3- 3 Spline used for Transverse –Hepatic Flexure Model (THF)..... 27

Fig. 3- 4 Mesh and Boundary conditions for the colonoscope insertion simulation 30

Fig. 3- 5 Input motion profile 31

Fig. 3- 6 Average kinetic energy and internal energy evolution for colon and SDC in RSJ model..... 34

Fig. 3- 7 Average kinetic energy and internal energy evolution for colon and SDC in RSF model..... 34

Fig. 3- 8 Average kinetic energy and internal energy evolution for colon and SDC in THF model..... 34

Fig. 3- 9 Ratio of kinetic energy to internal energy for colonoscope and colon in RSJ model..... 35

Fig. 3- 10 Ratio of kinetic energy to internal energy for colonoscope and colon in RSF model..... 35
Fig. 3- 11 Ratio of kinetic energy to internal energy for colonoscope and colon in THF model..... 36
Fig. 5- 1 Final colon deformation(cm) in RSJ (D=36 mm) 47
Fig. 5- 2 Colon deformation in RSJ (D=36 mm)..... 47
Fig. 5- 3 Three positions (a, b and c) of PDC in RSJ (D=36 mm) 47
Fig. 5- 4 Colon deformation under different contact friction coefficients in RSJ 49
Fig. 5- 5 Final colon deformation for different contact friction coefficient (u=0.05, 0.1) 49
Fig. 5- 6 Colon deformation induced by UTC, PDC and SDC in RSJ (D=23 mm)..... 51
Fig. 5- 7 Deformation of colon (D=23mm and D=36mm) induced by UTC, PDC and SDC..... 52
Fig. 5- 8 Final sigmoid colon deformation in RSF model 54
Fig. 5- 9 Sigmoid colon deformation in RSF model (α= 0°) 56
Fig. 5- 10 Sigmoid colon deformation in RSF model (α= 30°) 56
Fig. 5- 11 Sigmoid colon deformation in RSF model (α= 45°) 57
Fig. 5- 12 Final transverse colon deformation for THF model..... 58
Fig. 5- 13 Transverse colon deformation in THF model (β=0°)..... 60
Fig. 5- 14 Transverse colon deformation in THF model (β=30°)..... 60
Fig. 5- 15 Transverse colon deformation in THF model (β=45°)..... 61
Fig. 5- 16 Colonoscope buckling shape for fixed THF model 64

Fig. 5- 17 Colonoscope distal end displacement in fixed THF model (β= 0°) 65

Fig. 5- 18 Colonoscope distal end displacement in fixed THF model (β= 30°) 65

Fig. 5- 19 Colonoscope distal end displacement in fixed THF model (β= 45°) 66

Fig. 5- 20 Contact force in fixed THF model (β=0°) 66

Fig. 5- 21 Contact force in fixed THF model (β= 30°) 67

Fig. 5- 22 Contact force in fixed THF model (β= 45°) 67

List of Tables

Table 3- 1 Number of elements and nodes for Colon Models 28

Table 3- 2 Number of elements and nodes for Colonoscope Models 28

Table 3- 3 Mean duration for the insertion simulation 33

Table 5- 1 Colon deformation and relative difference at point A 52

Table 5- 2 Colon deformation and relative difference at point C 53

Table 5- 3 Differences of final sigmoid colon deformation induced by SC colonoscopes with respect to that induced by SDC for RSF model 55

Table 5- 4 Differences of final transverse colon deformation induced by SC colonoscopes with respect to that induced by SDC for THF model 59

CHAPTER I

INTRODUCTION

1.1 Research Background

1.1.1 Anatomy and Constraints of Colon

The human colon is held in place by peritoneum, a thin layer of tissue that supports the abdominal organs. It mainly consists of rectum plus sigmoid colon, descending colon, splenic flexure, transverse colon, hepatic flexure and ascending colon plus cecum as shown in Fig. 1- 1 (Blausen.com staff (2014)).

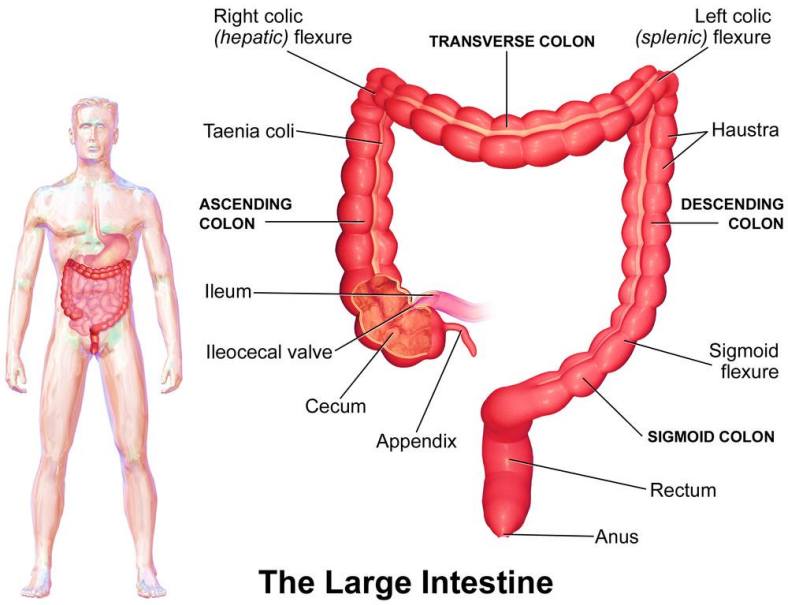

Fig. 1- 1 Human colon anatomy

The parts of the colon are either intraperitoneal or behind it in the retroperitoneum. Retroperitoneal organs in general do not have a complete covering of

peritoneum, so they are fixed in location. Intraperitoneal organs are completely surrounded by peritoneum and are therefore mobile. As to the colon, the ascending colon, descending colon and rectum are retroperitoneal while the transverse colon and sigmoid colon are intraperitoneal (American Accreditation HealthCare Commission). Therefore, the ascending colon, descending colon and rectum should be considered as fixed at their locations while the shape of sigmoid and transverse colon are flexible.

1.1.2 Colonoscopy Procedure and Patient Pain

A colonoscopy is a sensitive test which has both diagnostic and therapeutic functions (Rex DK et al. (2002); Brenner H. et al. (2014)). During the screening procedure, a thin and flexible tube called a colonoscope is inserted into the human large intestine to view and examine the entire colon, perform a biopsy or remove the premalignant polyps (Ferlay J. et al. (2012)). Colonoscopies are very important for human health. However, many risks are associated with the procedure, among which patient pain is one of the most serious contributing to the failure of a complete colonoscopy (Nishihara R. et al. (2012); Keswani, R. et al. (2012); Mitchell, R. et al. (2002)).

1.1.3 Technical Affecting Factors on Patient Pain

Technically, there are two factors which may affect the patient's pain during the procedure, including the skills of the endoscopist and the properties of the colonoscope itself. To improve the performance of the doctor and reduce the patient's pain, many designs focusing on preventing the loop formation which contributes to the excessive

stretching of colon wall, have been developed. These include over-tube colonoscope, variable stiffness colonoscope, image-guided scopes and self-propelled instruments methods. Choi, J., & Drozek, D. (2012) used embedded bending sensors to detect the endoscopic looping during the procedure. As for the influence of the properties of the colonoscope on patient's pain during a colonoscopy, (Loeve, A. et al. (2013)) reported that the stretching of the colon wall induced by the scope is the main origin of the patient comfort during a colonoscopy. Meanwhile, colon deformation induced by the scope consists of two different types: (1) colonoscope tip induced colon deformation. By using only straightforward insertion manipulation, the scope tip will eventually contact the bend or angulation in the outer curve. Fig. 1- 2 (Loeve, A. et al. (2013)) describes the push force distribution ($q_{push\text{-}1}$) on the colon wall during the interaction between the scope tip and the colon. At first stage, bend enlargement is mainly caused by moving the colon. The normal force ($q_{push\text{-}1}$) exerted by the scope tip on the colon wall. At second stage, with the further advancement of the scope, the magnitude of ($q_{push\text{-}1}$) increases. When the second bend has no more length to offer, the colon must stretch to enable further enlargement of the first bend. At the same time, deformation stresses in the colon wall grow due to the increasing stretching of the colon and these stresses begin to equal the push force and guide the scope along the bend. In the third stage, the tip has passed through the first bend. The stresses in the colon wall and the push forces exerted by the scope on the colon wall are now in equilibrium. The bend length of the scope and the force required to bend it is constant. The scope follows the bend without further stretching the bend. (2) colonoscope shaft induced colon deformation, which occurs due to the buckling of the flexible colonoscope shaft. The most common scenarios for this

type of patient's discomfort are that the stretching of the mobile sigmoid and transverse colonic tissue by the colonoscope shaft when the scope tip approaches the splenic and hepatic flexure respectively (Keswani, R. et al. (2012)). Fig. 1- 3 (Loeve, A. et al. (2013)) illustrates the deformation of the sigmoid colon induced by the scope shaft. When trying to advance the scope through the splenic flexure, the scope can bend or buckle when it is not sufficiently straight or guided.

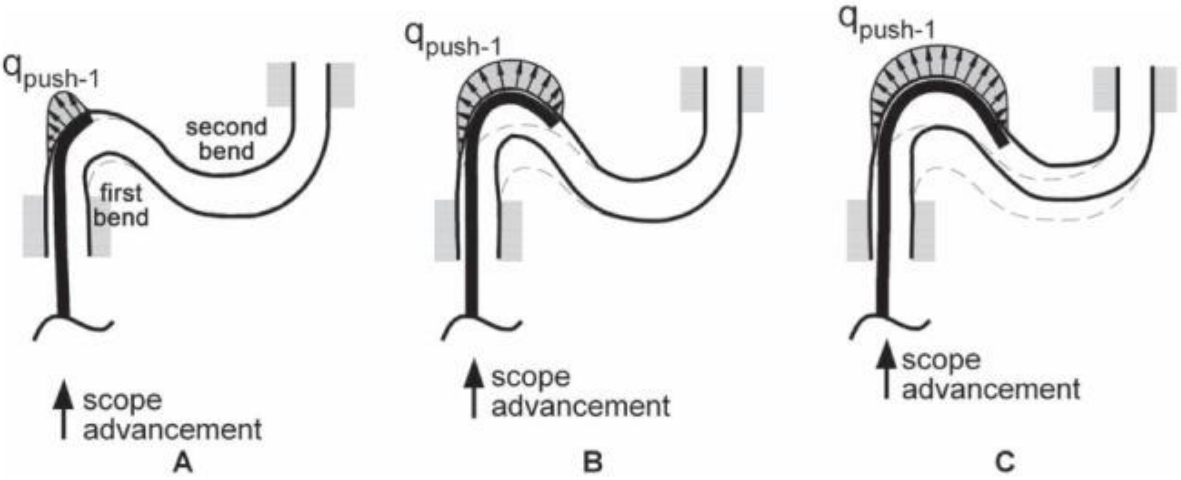

Fig. 1- 2 Three stages of colonoscope advancement through the angulation of the sigmoid colon

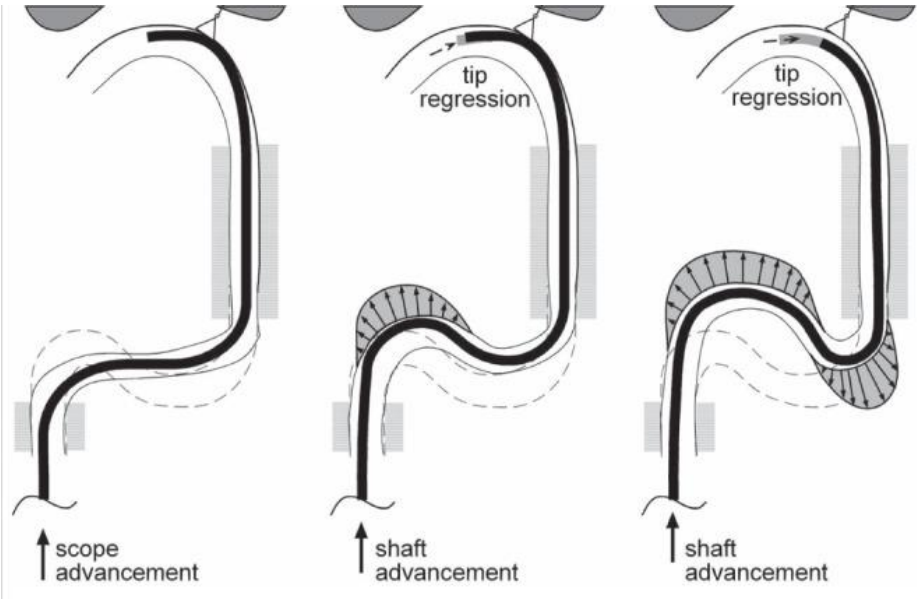

Fig. 1- 3 Sigmoid colon deformation induced by the scope shaft

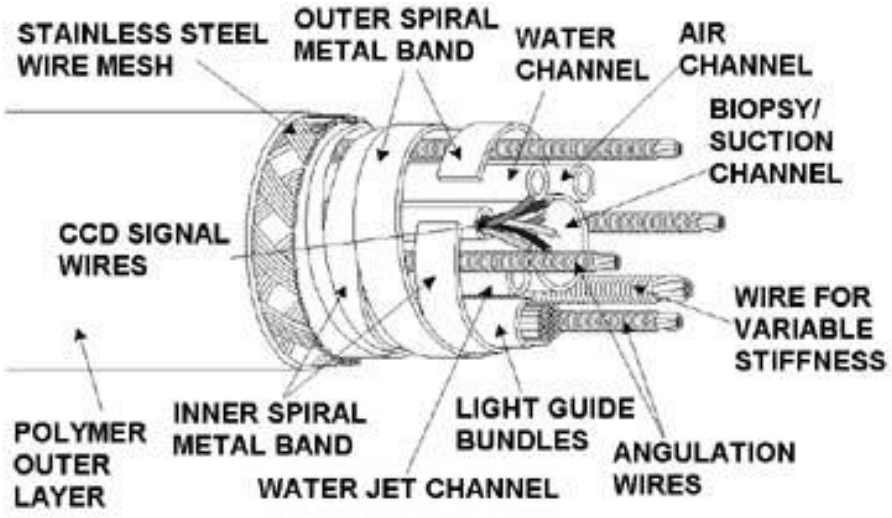

Fig. 1- 4 The structure of colonoscope insertion tube

To perform screening and therapeutic manipulations by the colonoscope, the insertion tube of the colonoscope contains many internal components. Fig. 1- 4 (Y.K. Chen & M.E. Powis. (2002)) illustrates the internal structure of the insertion tube of the colonoscope, it includes one or two instrument channel(s), one or two light guide bundles

(incoherent fiber optic), an air channel, a water channel, either an image guide bundle (coherent fiber optic) or a CCD chip with wire connections, and angulation wires. Due to the space required for the internal components of the colonoscope, a standard colonoscope (SDC) whose outer diameter is 12.8mm has been used for a very long time. Recently, small-caliber (SC) colonoscopes including 9.2mm ultrathin colonoscope (UTC) and 11.3mm pediatric colonoscope (PDC) have been developed ((Kozarek RA et al. (1989), Saifuddin T et al. (2000), Marshall JB et al. (2002), Park CH. Et al. (2006), Wehrmann T et al. (2008)). It is true that a SC colonoscope possess a more flexible shaft which may account for easier negotiation of the turn and angulation of the colon than the SDC. However, there are two reverse sides: (1) a SC colonoscope may cause a smaller contact area with the colon wall during interaction, (2) a more flexible shaft also means an easier buckling shaft.

1.1.4 Randomized Controlled Trials

To evaluate the efficacy of SC colonoscopes in reducing patient pain compared with that of SDC, several randomized controlled trials (RCTs) were conducted ((Marshall JB et al. (2002); Park CH et al. (2006); Farraye FA et al. (2004), Sato K (2013); Garborg KK et al. (2012); Tox U et al. (2013); Chen PJ. et al. (2008)). Nevertheless, these RCTs showed varying results, with some showed benefits with the use of SC colonoscopes whereas others did not. Among these RCTs, the characteristics of patients (gender, age and region) recruited were varied. Marshall JB et al. (2002) and Farraye FA et al. (2004) conducted the trials for female patients and the results showed the reduction of patient pain with the use of SC colonoscopes. The study conducted by Garborg KK et al. (2012)

for patients (43% female) also showed lower pain scores in the SC colonoscope group compared with the standard group. The studies from Saifuddin T et al. (2000) and Nemoto, D et al. (2017) showed the potential benefit of the ultrathin colonoscope in older patients. Sato K. et al. (2013) compared the efficiency of an ultrathin colonoscope with a SDC in female and male Japanese patients. The result suggested that the use of the SC colonoscope reduced pain in females while offering no advantage over a standard colonoscopy in male patients. However, the SC colonoscope used in this study was equipped with the design of passive bending and high force transmission. Contrary to the result in Sato K et al (2013), Luo DJ et al (2012) investigated the patient discomfort introduced by an ultrathin and a standard colonoscope for Chinese patients during a colonoscopy and found that the mean patient pain score was similar. The trial conducted by Chen PJ. et al. (2008) also showed no advantage with the use of PDC in reducing patient discomfort compared with the SDC. Based on above findings, an assumption was made, i.e, the efficacy of the SC colonoscopes in reducing patient pain may be affected by the patient characteristics in terms of gender, age and region. However, whether such an assumption is reasonable is still unclear due to many disturbing factors. Generally, these disturbing factors can be classified into 3 aspects: 1) the insufflation methods (air, water, CO_2 immersion, and water exchange), which have been reported to be able to affect the outcome, were varied among RCTs (Jia, Hui. Et al. (2017), Hsieh, Y. H et al. (2017) and Kim, Sy et al. (2017)); 2) apart from a smaller diameter shaft, the SC colonoscopes used in some RCTs were also equipped with some new technical features, including a high force transmission shaft, a variable stiffness shaft or a passive bending. These have been proved to be helpful in reducing patient pain through researches

(Rajagopalan, R et al. (2013); Pasternak et al. (2017)); 3) The endoscopists were not blinded to the colonoscope, thus, their skills may largely affect the result. Usually, the last disturbing factor exists in all RCTs and could not be avoided. Such s limitation makes it difficult to investigate the influence of patient characteristics on the performance of SC colonoscopes in terms of reducing patient pain through RCTs.

1.2 Research Motivation

To explore the influence of gender, age, and region of patients on the efficacy of SC colonoscopes in reducing patient pain, a numerical model could provide such insight is developed in our work. Finite element modeling is employed to simulate the insertion of the colonoscope in colon models. Patient pain is predicted through comparing the colon deformation during the insertion simulation. Such a model could also overcome the limitation of RCT, i.e. the skill of endoscopist.

1.3 Scope

The model developed in this research aims to simulate the insertion process of colonoscopes in colon models. Patient pain induced by the colonoscope is predicted and compared based on colon deformation during the insertion simulation. To account for the anatomic difference for human colon in terms of gender, age and region, 3 different colon segments with different angles, curvatures, diameters and contact friction coefficients were modelled. At the same time, three different diameters for colonoscopes, including 12.8 mm for SDC, 11.3mm for PDC, and 9.2mm for UTC were used. The experiment was carried out to determine the experimental response of a porcine colon under tensile

loading. An optimized procedure with the use of the ANSYS and Optislang programs was developed to provide the essential hyperelastic parameters for colon tissue material model.

The thesis is arranged as follows: Chapter II covers a literature review on the anatomical differences of human colon in terms of gender, age and region, the selection of FEM solver and constitutive modelling of colon tissue; Chapter III describes the methodology used for conducting the insertion simulation. The experimental set-up and parameters optimization procedures which provide the essential parameters for Chapter III is presented in Chapter IV. All the results are presented in Chapter V. Conclusions are reached and future recommendations of this research are offered in Chapter VI.

CHAPTER II

REVIEW OF LITERATURE

The purpose of this chapter is to provide a basis for this study by reviewing literature that is pertinent to the goals and objectives of this research. The topics of literature reviews are previous work about the modeling of the interaction between colon and colonoscope, the anatomic characteristics of human colons considering effects of age, region and gender, the comparison between implicit and explicit FEM solution method, and the constitutive modelling of colon tissue.

2.1 Previous Work

By doing literature reviews, two studies conducted by Jung, H et al. (2012) And W B Chen et al. (2013) focused on modeling the interaction between colon and colonoscope during a colonoscopy. Jung, H et al. (2012) proposed a novel simulation framework for real-time deformation of the colon and colonoscope, using a skeleton-driven deformation method. Cylindrical lattices and a center-line were employed as the skeletons, and a mass-spring model was applied to the skeletons for the mechanics-based simulation. The center-line-based collision detection and resolution algorithm was proposed to simulate the interaction between the colon and endoscope. A haptic rendering algorithm using the energy method was proposed to produce feedback force, based on physical interaction between the colon and colonoscope. Such a method could provide real time deformation of the colonic tissue induced by the colonoscope during a

colonoscopy. However, only elastic or viscoelastic properties of the colon tissue can be characterized with the use of mass-spring model, which limited the accuracy of simulation results. In the research conducted by W B Chen et al. (2013), contact force computation was formulated into a linear complementarity problem (LCP) by linearizing Signorini's problem, which was adapted into non-interpenetration with unilateral constraints. Frictional force was computed by the mechanical compliance of implicit finite element method (FEM) models with the consideration of dynamic friction between the colonoscope and the intestinal wall. Furthermore, a mathematical model of the elongation of the colon that predicts the motion of scope relative to the intestinal wall in colonoscopy was presented. Such a method could provide real time shape of the colonoscope. Nevertheless, the colon was modelled as an elastic Timoshenko hollow cylinder and the deformation of colon induced by the colonoscope was considered to uniformly distribute along the circumferential direction when doing calculation, which limited the accuracy of simulation results.

2.2 Anatomic Characteristics of Human Colons

As for the gender based structural difference for the human large intestine. Saunders et al. (1996) investigated the colonic length and mobility for female and male colon. The experiments were independently taken by two physicians who were unaware of each patient's gender and the results showed that although there were no significant differences in rectum plus sigmoid, descending, or ascending plus cecum segmental lengths, women had longer transverse colons. At the same time, there were no differences in mobility of the descending colon and transverse colon between the sexes, but the

transverse colon reached the true pelvis more often in women than in men. Rowland, R et al. (1999), Streett, S (2007 and Todd N Witte, & Robert Enns. 2007 studied the issue of sex differences contributing to colonoscopy difficulty and found that apart from the longer transverse colon, the female has deeper pelvis than male, which creates the potential for lower retroperitoneal fixation of descending colon in the pelvis.

The anatomic difference related to age for the human colon have been conducted for many clinical researches (Nivatvougs, S et al. 1982; Ravi J et al.1988; Waye, & Bashkoff. 1991; Saunders et al. 1996; Schmidt CM et al. 1994; Church JM et al. 1994). It was reported that older female patients were suffered from more diverticular diseases than young patients before doing colonoscopies. As a result, those older patients were prone to have a fixed, and angulated sigmoid colon due to prior pelvic surgeries. Also, the diverticular diseases are responsible for bowel obstruction, which may in turn increase the contact friction between the internal surface of colon and colonoscope during colonoscopy.

Watters, D et al. (1985) examined the mechanical properties of large intestine taken from European and African subjects and found that the average internal diameter of colons for European are 23mm and 36mm for African. Such difference could represent the region induced structural difference for human colon.

2.3 Finite Element Solution Method

Finite element software employs numerical integration methods for the solution of partial differential equations. The Numerical solution schemes are often classified as being implicit or explicit. These two methods have their own applicability and

advantages in terms of computational cost, accuracy and stability to a particular problem. Therefore, it's critical to select a suitable finite element solution method for the problem before doing the simulation.

The primary differences between implicit and explicit method are different time integration methods and solution methods they are using. Among numerical integration methods, the implicit method applies Newmark time integration method while explicit method uses central difference time integration method. As for the implicit nonlinear dynamics solutions, the Newton-Raphson solution method is employed to update the effective stiffness matrix. The following section thoroughly demonstrates and compare the attributes of both implicit and explicit method, summarized from Cook, R. D et al (1981), Fagan (1992), Bathe, K. J (1982), the Abaqus Theory Manual (Abaqus, 2011), Theoretical Manual (LS-DYNA, 2013), Advanced Analysis Techniques Guide (ANSYS, 2009) and Rust, W &Schweizerhof, K. (2003).

2.3.1. Introduction to Implicit Finite Element Solution Method

For linear structural dynamics systems, the internal load is linearly proportional to the nodal displacement, and the structural stiffness matrix remains constant, the spatial discretization of the structure leads to the governing equilibrium equation of structural dynamics, and can be expressed as (2.1)

$$[M]\{\ddot{U}\}+[D]\{\dot{U}\}+[K]\{U\}=\{F\} \tag{2.1}$$

Where

$[M]$ = Mass Matrix; $[D]$ = Damping Matrix; $[K]$ = Stiffness Matrix

$\{F\}$ = Force Vector

$\{U\}$ = Column Matrix of Displacements corresponding to Force Vector

$\{\dot{U}\}$ = Velocity Vector

$\{\ddot{U}\}$ = Acceleration Vector

The Newmark method expressed the velocities and displacements at the end of a time increment Δt in terms of the known parameters at the beginning and the unknown acceleration at the end of the time step as (2.2) and (2.3):

$$[M]\{\ddot{U}_{i+1}\}+[D]\{\dot{U}_{i+1}\}+[K]\{U_{i+1}\}=\{F_{i+1}\} \tag{2.2}$$

$$U_{i+1}=U_i+\dot{U}_i\Delta t+\left[(\frac{1}{2}-\beta)\ddot{U}_i+\beta\ddot{U}_{i+1}\right]\Delta t^2 \tag{2.3}$$

Where

α and β are numerical integration parameters

$\Delta t = t_{i+1}-t_i$

$U_i,\ \dot{U}_i,\ \ddot{U}_i =$ Displacement, Velocity and Acceleration at time t_i

$U_{i+1},\ \dot{U}_{i+1},\ \ddot{U}_{i+1} =$ Displacement, Velocity and Acceleration at time $t_{i+}\Delta t$

In solving the displacement, velocity and acceleration at time $t_{i+}\Delta t$, the equilibrium equation (2.1) can be rewritten as:

$$[M]\{\ddot{U}_{i+1}\}+[D]\{\dot{U}_{i+1}\}+[K]\{U_{i+1}\}=\{F_{i+1}\} \tag{2.4}$$

By making use of the three algebraic equations given in (2.2) through(2.4), a single time integrator in terms of the unknown displacement U_{i+1} at time $t_{i+}\Delta t$ and the three known quantities U_i, $\dot{U}_i$ and $\ddot{U}_i$ can be expressed as:

$$(a_0[M]+a_1[C]+[K])U_{i+1} = F_{i+1}+[M](a_0U_i+a_2\dot{U}_i+a_3\ddot{U})+[\mathrm{C}](a_1U_i+a_4\dot{U}_i+a_5\ddot{U}) \quad (2.5)$$

Where

$$a_0=\frac{1}{\alpha\Delta t^2};\ a_1=\frac{\beta}{\alpha\Delta t};\ a_2=\frac{1}{\alpha\Delta t};\ a_3=\frac{1}{2a}-1$$

$$a_4=\frac{\beta}{a}-1;\ a_5=\frac{\Delta t}{2}(\frac{\beta}{a}-2);\ a_6=\Delta t(1-\beta);\ a_7=\beta\Delta t$$

First, the unknown displacement U_{i+1} at time $t_{i+}\Delta t$ is calculated using Equation (2.5). Then, two unknowns $\dot{U}_{i+1}$ and $\ddot{U}_{i+1}$ are computed by using the following equations:

$$\dot{U}_{i+1}=a_1(U_{i+1}-U_i)-a_4\dot{U}_i-a_5\ddot{U}_i \quad (2.6)$$

$$\ddot{U}_{i+1}=a_0(U_{i+1}-U_i)-a_2\dot{U}_i-a_3\ddot{U}_i \quad (2.7)$$

Matrix $(a_0[M]+a_1[C]+[K])$ in equation (2.5) is generally referred to as the effective stiffness matrix $[K]^{eff}$.

$$[K]^{eff}=(a_0[M]+a_1[C]+[K])U_{i+1}$$

For linear cases, the effective stiffness matrix remains constant in all the computational steps unless the time step is changed. The parameter α and β determine the integration accuracy and stability. When α=1/2 and β= 1/4, equation (2.6) and (2.7) correspond to constant average acceleration method (Zienkiewicz, O. C. 1977). The method is implicit and unconditionally stable.

Nonlinear Structural Case

For a nonlinear analysis, the internal load is no longer linearly proportional to the nodal displacement, and the effective stiffness changes at every time step and is

displacement dependent. Most commercial finite element software employs the Newton Raphson solution method, along with implicit Newmark time integration methods to provide solution for nonlinear structural problems.

Instead of Equation (2.1), the governing equilibrium equation for nonlinear structural problem should be written as Equation (2.8) :

$$[M]\{\ddot{U}\}+[D]\{\dot{U}\}+\{F^{i}\}=\{F^{a}\} \tag{2.8}$$

Where

$\{F^{i}\}$ =Internal Force vector

$\{F^{a}\}$ = External Applied Boundary Conditions and/or Force vector

The Newmark time integration method assumes that at the time $t_{i+}\Delta t$, the equation of motion given in (2.9) can be rewritten as:

$$[M]\{\ddot{U}_{i+1}\}+[D]\{\dot{U}_{i+1}\}+\{F^{i}{}_{i+1}(\{U_{i+1}\})\}=\{F^{a}{}_{i+1}\} \tag{2.9}$$

Where

$\{F^{i}{}_{i+1}(\{U_{i+1}\})\}$ represents that the internal force at time $t_{i+}\Delta t$ is dependent on the displacement U_{i+1}.

$\{\dot{U}_{i+1}\}$ and $\{\ddot{U}_{i+1}\}$ can be updated using Newmark time integration algorithms as given in Equations (2.6) and (2.7)

By introducing the residual vector $\{R_{i+1}(\{U_{i+1}\})\}$, Equation (2.9) can be written as:

$$\{R_{i+1}(\{U_{i+1}\})\}=\{F^{a}{}_{i+1}\}-\{F^{i}{}_{i+1}(\{U_{i+1}\})\}-[M]\{\ddot{U}_{i+1}\}-[D]\{\dot{U}_{i+1}\} \tag{2.10}$$

In general, for non-linear problems, At the end of each increment, the structure of the non-linear geometries, materials, constitutive laws and/or boundary conditions may have changed and therefore equation (2.9) must be updated to represent this. After each increment of an implicit analysis, the analysis performs Newton-Raphson iterations from time t_i to $t_{i+}\Delta t$ to solve for all nodal displacements U_{i+1} to enforce equilibrium of the internal structure forces with the externally applied boundary conditions and/or loads. a linearized form of the time integration operator can be obtained by the Newton-Raphson method, such that for the k^{th} iteration:

$$\left\{R_{i+1}(\{U_{i+1}^k\})\right\} + \frac{\partial\left\{R_{i+1}(\{U_{i+1}^k\})\right\}}{\partial U_{i+1}^k}\left\{\Delta U_{i+1}^k\right\} = \{0\} \tag{2.11}$$

Where:

$\{U_{i+1}^k\}$ = the estimate of $\{U_{i+1}\}$ at the k^{th} iteration

$\left\{\Delta U_{i+1}^k\right\}$ =the displacement increment of $\{U_{i+1}\}$ at the k^{th} iteration

The following equation can be obtained by substituting Equation (2.10) into Equation (2.11):

$$\left[(a_0[M] + a_1[\mathrm{D}] + [K_{i+1}^k(\{\mathrm{U}_{i+1}^k\})]\right]\left\{\Delta U_{i+1}^k\right\} = \left\{R_{i+1}(\{U_{i+1}^k\})\right\} \tag{2.12}$$

Where

$$a_0 = \frac{1}{\alpha\Delta t^2}$$

$$a_1 = \frac{\beta}{\alpha\Delta t}$$

$[K_{i+1}^k(\{\mathrm{U}_{i+1}^k\})]$ = the tangent stiffness matrix at time $t_{i+}\Delta t$

$[(a_0[M] + a_1[C] + [K_{i+1}^k(\{\mathrm{U}_{i+1}^k\})]$ = effective stiffness matrix

Equation (2.12) must be solved for each iteration for the change in incremental displacements, $\left\{\Delta U_{i+1}^{k}\right\}$, In order to solve for $\left\{\Delta U_{i+1}^{k}\right\}$, the effective stiffness matrix must be inverted.

The accuracy of the solution is also dictated by the convergence criterion where the updated value for $\{R_{i+1}(\{U_{i+1}\})\}$ must be less than a tolerance value. Complications can arise in an analysis that has a highly non-linear stress-strain response or where there is contact and sliding between two surfaces. In such cases many iterations are usually needed to solve for an increment leading to progressively smaller time steps being used. If large nonlinearities are encountered, convergence may be impossible to achieve in practical terms.

2.3.2. Introduction to Explicit Finite Element Solution Method

The explicit procedure is based on the implementation of an explicit integration rule along with the use of diagonal element mass matrices. The equation of motion for the body is integrated using an explicit central difference integration rule:

$$\ddot{U}_i = \frac{1}{\Delta t^2}(U_{i-1} - 2U_i + U_{i+1}) \tag{2.13}$$

$$\dot{U}_i = \frac{1}{2\Delta t}(U_{i+1} - U_{i-1}) \tag{2.14}$$

Which include the states at time t, $t_{i+}\Delta t$, and $t_{i-}\Delta t$.

Linear Structural Case

For the linear dynamic structural problem, the governing equilibrium equation at time t_i can be expressed as:

$$[M]\{\ddot{U}_i\}+[D]\{\dot{U}_i\}+[K]\{U_i\}=\{F_i\} \tag{2.15}$$

Substitutes (2.13) and (2.14) into (2.16) and we can have:

$$\left[\frac{1}{\Delta t^2}[M]+\frac{1}{2\Delta t}[D]\right]\{U_{i+1}\}= \tag{2.16}$$
$$\{F_i\}-\left[[\mathrm{K}]+\frac{2}{\Delta t^2}[\mathrm{M}]\right]\{U_i\}-\left[\frac{1}{\Delta t^2}[\mathrm{M}]+\frac{1}{2\Delta t}[\mathrm{C}]\right]$$

From (2.16), displacement $\{U_{i+1}\}$ at time $t_{i+}\Delta t$ is determined by displacement $\{U_i\}$ at time t_i. Also, there is no stiffness matrix of complete assemblage needs to be inverted and only matrix multiplications are required.

However, the effectiveness of the central difference method depends on efficient performance of each time step solution. Equation (2.16) demonstrates that the smaller the value of the time increment Δt, the more accurate the solution. As a result, a large amount of time steps usually are needed.

Nonlinear Structural Case

For nonlinear problem, the equation of motion at time t_i can be expressed as:

$$[M]\left\{\ddot{U}_i\right\}+[D]\left\{\dot{U}_i\right\}+\left\{F^i{}_i(\{U_i\})\right\}=\left\{F^a{}_i\right\} \tag{2.17}$$

Where

$\left\{F^i{}_i(\{U_i\})\right\}$ =Internal force

$$F^i=\sum(\int_V \beta^N \sigma dV+F^{hg})+F^{contact}$$

V is the current volume of the model.

$\sigma(x)$ is the stress at a point currently located at position x.

$\beta^N(x)$ is the strain rate-displacement rate transformation defined from the interpolation assumption in the element $\dot{\varepsilon} = \beta^N \dot{u}^N$.

F^{hg} is the hourglass force

$F^{contact}$ is the contact force

Therefore, the accelerations are computed directly at time t_i as:

$$[M]\{\ddot{U}_i\} = \{F^a{}_i\} - \{F^i{}_i(\{U_i\})\} - [D]\{\dot{U}_i\} \tag{2.18}$$

For the nonlinearities, the equation (2.18) are uncoupled, and can be solved directly (explicitly) without any iteration and the stiffness matrix [K] does not need to be inverted. All the nonlinearities (including contact) are included in the internal force vector. The major computational expense is in calculating internal forces, and CPU cost is approximately proportional to the size of the finite element model and does not change as dramatically as it does in the implicit method.

2.3.3. Selection of Finite Element Solution Method

The Research conducted W B Chen et al. (2013) showed that the interaction between colon and colonoscope during colonoscopy are multi-body non-interpenetration contact problem. Also, the deformation of colon shows nonlinear properties. Explicit finite element solution methods are more efficient at handling large numbers of contacts than implicit methods, as an explicit solver solves for the solution directly and it does not require multiple iterations and inversion of stiffness matrix. For this reason, the choice of an explicit solver was deemed appropriate. Additionally, previous similar studies of the

insertion simulation of a guidewire inside the artery used an explicit code (Kalaji, A et al. (2013); Duménil, A. et al. (2013); J. Gindre, A et al. (2015))

Therefore, in this research, the explicit finite element solution method is selected. The insertion procedures of colonoscopes inside the colon model were performed using the ANSYS LS-DYNA Explicit 17.0 finite element solver on a Dell laptop equipped with one 4-core Intel® i7-4600U CPU (2.10GHz) processor.

2.4 Constitutive Modelling of Colon Tissue

To compare and predict the patient pain induced by the colonoscope, an accurate modelling of colon deformation is required. Colon is a thin-walled tubular like soft tissue, which mainly subjects to the tensile force by the colonoscope during colonoscopy. Many investigations have focused on gaining insight into the mechanical response of the colon tissue under tensile loading (Egorov. et al. 2002; Carniel, E. L., et al. 2014; Christensen, M. et al. 2015; Massalou, Masson. et al. 2016). When subjected to small deformations (less than 2–5%), the mechanical behaviour of colonic tissue can generally be modelled adequately using conventional linear elasticity. However, under large deformations, colonic tissue exhibits highly nonlinear elastic behaviour due to rearrangements and reorientation of fibre directions and therefore a linear elastic model does not accurately describe its material behaviour. The theory of nonlinear elasticity using hyperelastic models describes the elastic nonlinear tissue response under large strains more accurately in comparison with the linear elasticity theory.

Although colonic tissues also possess visco-elastic behaviour and could not be considered as pure hyperelastic, an assumption of hyperelasticity allows a reasonable

estimation of the mechanical properties and it's suitable for characterizing the deformation of colon when the loss of strain energy is small due to the low loading rate of the colonoscope during a colonoscopy. Also, it is well established in the literature that non-linear hyperelastic isotropic material models are a good compromise between physical reality and computational efficiency when dealing with human-body soft tissue (Ní Ghriallais, R. &M. Bruzzi 2014).

The hyperelastic approach postulates an existence of the strain energy function (scalar function per unit reference volume) W, which relates the displacement of the tissue to the corresponding stress values. The strain energy function has a meaning of the energy stored by a system undergoing deformation. When the load is removed, strain energy is gradually released as the system returns to its original shape.

For homogeneous material, the strain energy function is a function only of the deformation gradient F defined as:

$$F = \frac{\partial x}{\partial X} \tag{2.19}$$

Where

x denotes a point in the current configuration

X denotes a point in the reference configuration

The right Cauchy-Green deformation tensor C is a measure of the strain the body experiences and is defined as

$$C = F^T F \tag{2.20}$$

For isotropic materials, the strain energy function $W=W(F)$ is a function of invariants $W=W(I_1, I_2, I_3)$, which are defined as:

$$I_1 = trace(C) = \lambda_1^2 + \lambda_2^2 + \lambda_3^2$$

$$I_2 = \frac{1}{2}(I_1^2 - trace(C^2)) = \lambda_1^2\lambda_2^2 + \lambda_1^2\lambda_3^2 + \lambda_2^2\lambda_3^2 \tag{2.21}$$

$$I_3 = \det(C) = \lambda_1^2\lambda_2^2\lambda_3^2$$

λ_1, λ_2 and λ_3 are the principal stretches of the deformation and often called the principal stretch ratios. Colonic tissue is also incompressible, which means the volume of the material remains constant during deformation. For incompressible materials, $\det(C) = \lambda_1^2\lambda_2^2\lambda_3^2 = 1$ and the strain energy function is, therefore, a function of only two invariants $W = W(\mathrm{I}_1, \mathrm{I}_2)$.

There are several forms of strain energy potentials available in ANSYS to model approximately incompressible isotropic hyperelastic materials including the neo-Hookean, Arruda-Boyce, Gent, Mooney-Rivlin, Ogden, polynominal, Yeoh and Ogden forms. Among these forms, Polynomial forms of the strain energy functions are the most popular in the constitutive modelling of biological tissues because of their simplicity and, therefore, calculation efficiency (Wex C. et al. 2015). The polynomial forms of the strain energy function include Neo-Hookean model, Mooney-Rivlin model, Ogden model and Yeoh model. In our work, a three-parameter Mooney-Rivlin model is selected to model the deformation of colonic wall due to the stretching of the colonoscope.

The strain energy for such a model is defined as:

$$W = C_{10}(I_1 - 3) + C_{01}(I_2 - 3) + \mathrm{C}_{11}(I_1 - 3)(I_2 - 3) + \frac{1}{d}(\mathrm{J}-1)^2 \tag{2.22}$$

Where C_{10}, $C_{01,}$ and C_{11} are the material stiffness constants corresponding to the elastic modulus in a linear material. $d=2/k$. where K is the bulk modulus.

$J=det(F)=\lambda_1\lambda_2\lambda_3$. For an incompressible material, J = 1.

Therefore, for incompressible material, W can be modified as

$$W = C_{10}(I_1 - 3) + C_{01}(I_2 - 3) + C_{11}(I_1 - 3)(I_2 - 3) \tag{2.23}$$

CHAPTER III

INSERTION SIMULATION

3.1 Geometry and Mesh

To account for the structural differences between the human colon in terms of gender, age and region, three segments of the human colon were selected and modeled: rectosigmoid junction (RSJ), rectum-splenic flexure segment (RSF) and transverse hepatic flexure segment (THF) models.

As an elementary study, based on the studies about colon anatomy from Whitmer et al. 2007, the idealized colon model was assumed as a thin-walled tube with uniform thickness and internal diameter in this work. The normalized lengths of descending and ascending colon are 10 cm, which were derived from Whitmer et al. (2007). The splenic and hepatic flexure were modelled as an arc with radius (R) equals to 5cm.

The average length of the centerline of a rectosigmoid junction (RSJ) is 15cm (Welch, C.R et al. (2016)). To study the ability of scope negotiating rectosigmoid junction, the idealized centerline of RSJ was defined by an arc of 180° with radius R=5 cm and 4cm straight section in the beginning of arc to model the rectum as shown in Fig. 3- 1.

As for RSF model, it is reported that the rectum and the descending colon lies approximately 20 cm apart from the research of Loeve, A et al. (2013). To account for change of the position of the fixation of the sigmoid-descending junction induced by

gender of the human, 20cm straight line with α=0°, 30° and 45° as shown in Fig. 3- 2 was selected to model the centreline of straightened sigmoid colon, respectively.

As for THF model, the transverse colon has a typical triangular configuration and is enveloped by the transverse mesocolon peritoneum. The degree of droop of the transverse colon towards the pelvis accounts for the variable bowel length, and influences the acuteness of the hepatic flexure bend. It is reported that for persons of normal body mass index, abdominal diameter should be under 25 cm (Ribarren et al. (2006)). At the same time, the mean abdominal wall thickness is 22 mm (Balaguru, D. et al. (2011)). Therefore, the straight distance between splenic and hepatic flexure was selected as 20 centimeters. An angle β was equipped with 0°, 30° and 45° to account for the change of curvature and length of the transvers colon as shown in Fig. 3- 3.

To study the influence of colon diameter (human colon size) on scope's behaviour, two different colon internal diameters: 23 mm for European patients and 36mm for African patients were selected and modelled for RSJ model.

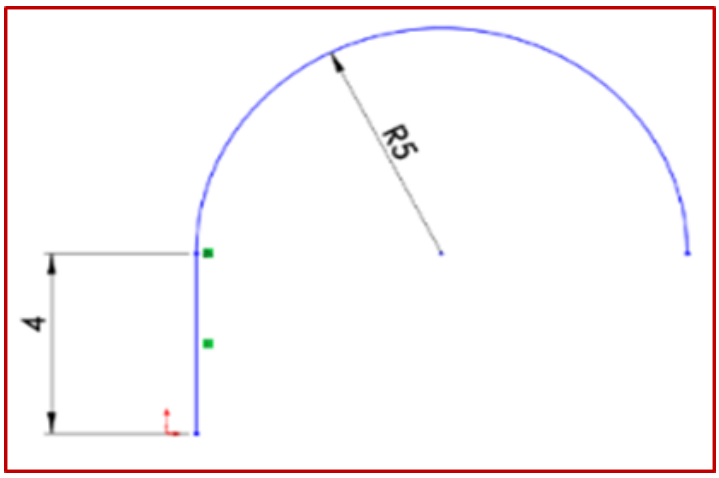

Fig. 3- 1 Spline used for Rectosigmoid Junction Model (RSJ)

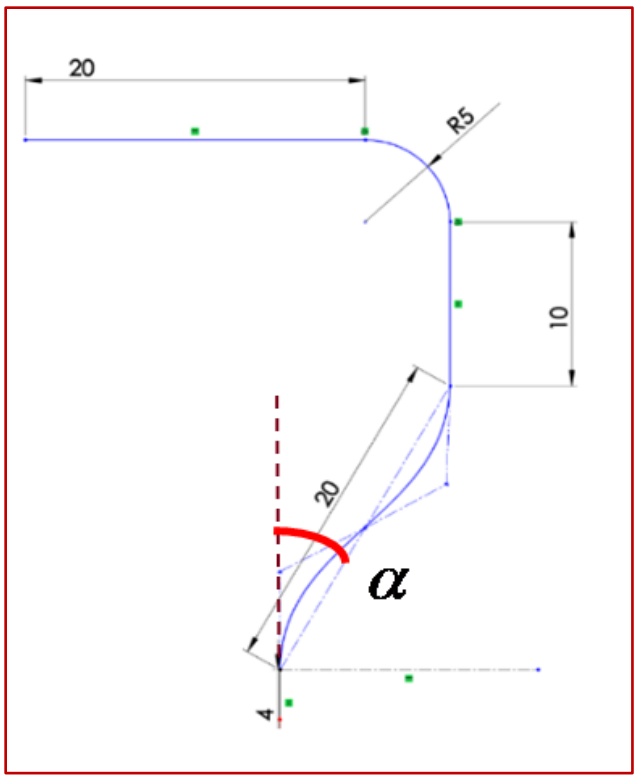

Fig. 3- 2 Spline used for Rectum-Splenic Flexure Model(RSF)

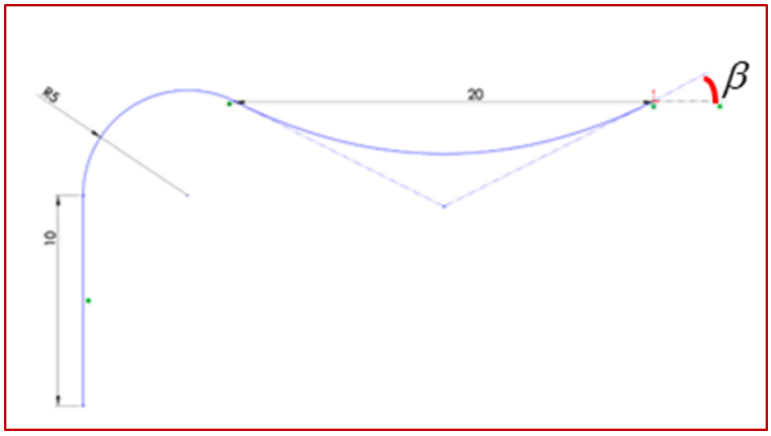

Fig. 3- 3 Spline used for Transverse –Hepatic Flexure Model (THF)

All colon models were meshed with Discrete Kirchhoff Triangular (DKT) triangular shell elements, whose characteristic size was 3mm as shown in Fig. 3- 4. The colonoscope was modelled as a cylinder with a hemisphere tip and meshed with 8 nodes brick element as shown in Error! Reference source not found.. Three different diameters

(13.3 mm SDC, 11.1mm PDC and 9.2 mm UTC) with length of 30cm for insertion simulation in RSJ model ,70 cm in RSF model, and 50cm in THF model were studied. Number of meshed nodes and elements for colon and colonoscope were summarized in Table 3- 1. Number of elements and nodes for Colon Models were summarized in Table 3- 2.

Table 3- 1 Number of elements and nodes for Colon Models

Model	RSJ D=23mm	RSJ D=36mm	RSF α=0°	RSF α=30°	RSF α=45°	THF β=0°	THF β=30°	THF β=45°
Number of nodes	2064	2792	6632	7208	8717	4086	5324	5977
Number of elements	4076	5504	13188	15674	17361	7832	9902	1115

Table 3- 2 Number of elements and nodes for Colonoscope Models

		UTC	PDC	SDC
Number of nodes	RSJ	4983	5145	12231
	RSF	11410	14996	25025
	THF	8208	8975	18975
Number of elements	RSJ	3750	3942	10650
	RSF	8775	12025	22032
	THF	6250	6921	17781

3.2 Material Properties

Since the mechanical stretch of colon induced by the colonoscope during the insertion process is mainly along its longitudinal direction, we chose to characterize the longitudinal behaviour of the colonic wall using the isotropic and incompressible three parameter-Mooney Rivlin hyperelastic model. The optimized material parameters for C_{10},

C_{01} and C_{11} are 652.01Pa, 42835.25Pa and 219120.3Pa, which were identified through an optimization procedure shown in CHAPTER IV . A density of $\rho = 1040 kg/m^3$ was applied for the colonic tissue (ICRU, 1992b).

As for the properties of the Colonoscope, the complex and sensitive internal components of colonoscope make it difficult to obtain the mechanical properties (Young's modulus) from stress-strain relationship like colon through tensile test. Therefore, the Young's modulus of colonoscope used for simulation in this paper was extracted from the flexural rigidity (EI) through 3-point bending test Conducted by Wu Bing et al. (2015). As a result, a linear elastic material model was applied for the colonoscope model with a Young's Modulus of E = 16MPa, a density of ρ = 2944 kg/m3 (Van Dam et al.2006), and a Poisson's ratio of ν = 0.3.

3.3 Boundary Conditions

The boundary constraints for colon and colonoscope are shown in Fig. 3- 4. The edge nodes at each end of the colon models and all the nodes comprising the rectum, descending colon, splenic flexure, hepatic flexure and ascending colon sections were fixed, which are marked with red line.

To prevent the buckling of the colonoscope before entering the colon model, a rigid sheath was introduced in our model. It is known that an experienced endoscopist always straighten the sigmoid and transverse colon by torqueing or pulling scope before pushing it to pass through the splenic and hepatic flexure to reduce the possibilities of loop formation (Loeve, A. et al. 2013). Therefore, there exists the dynamic relaxation of the colonoscope between the action of straightening sigmoid colon and reinsertion into

splenic flexure and hepatic flexure. To compare the colon deformation induced by the buckling shaft of the colonoscope when it negotiates the splenic and hepatic flexures. In our work, birth and death constrains were used to control both the lateral movement of sigmoid and transverse colon and the motion of scope to simulate such process. The input motion profile of insertion in RSJ, RSF and THF models as well as the birth and death constraining of the lateral movement of sigmoid and transverse colon in RSF and THF are shown in Fig. 3- 5. Also, such a birth and death Constraints could ensure the same straightening process and thus eliminating the disturbing factor, i.e., endoscopists' skill.

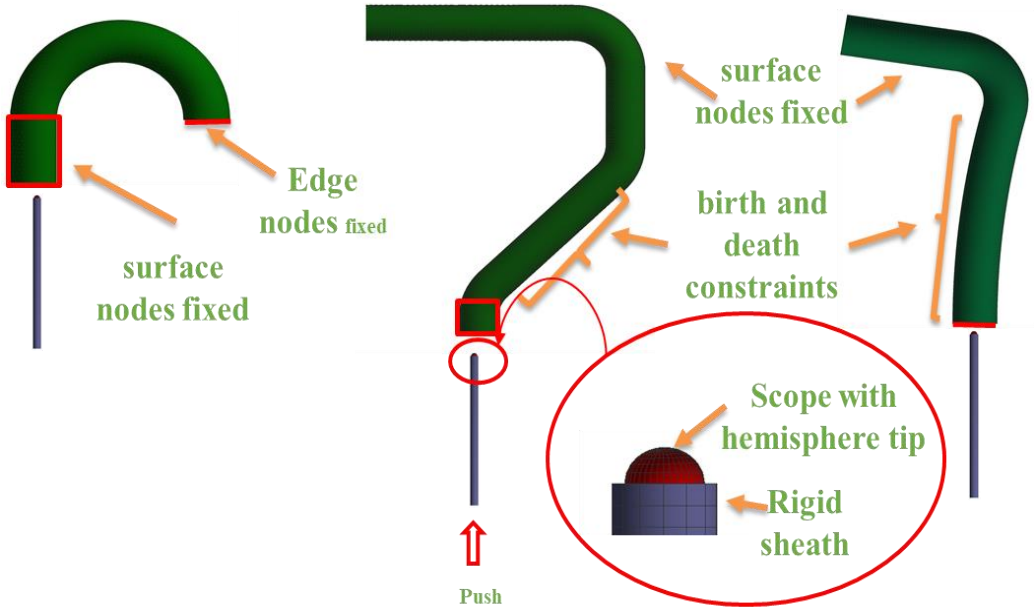

Fig. 3- 4 Mesh and Boundary conditions for the colonoscope insertion simulation

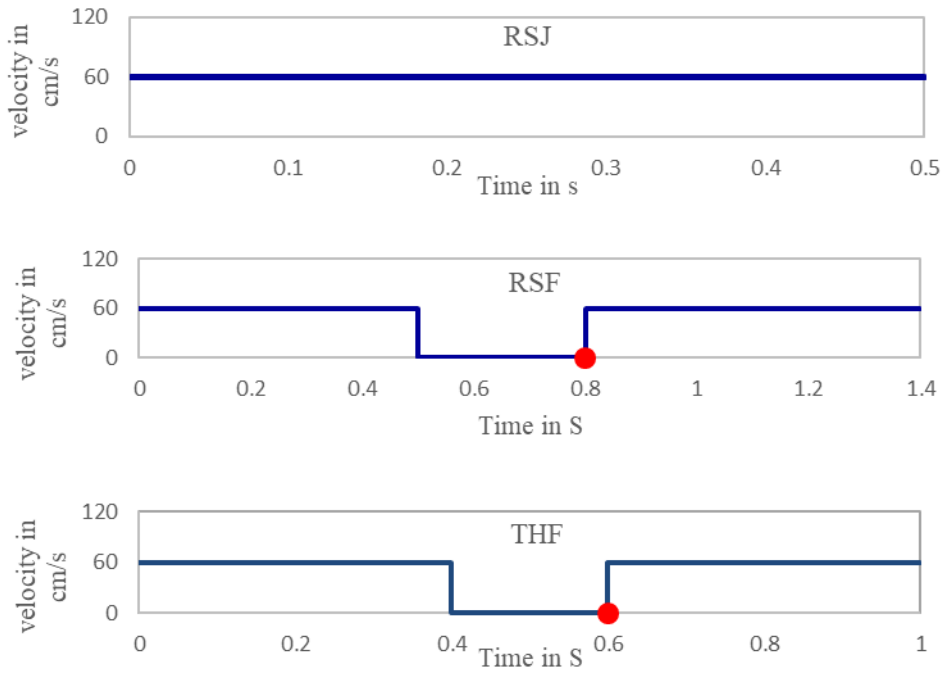

Fig. 3- 5 Input motion profile

3.4 Quasi-Static Modelling

The colonoscope was pushed into colon models by prescribing a ramp motion function with a constant velocity to the set of nodes located at their lower end as shown in Fig. 3- 4 and Fig. 3- 5.

It is known that the colonoscopy is a quasi-static clinical process, hence, inertia effects have to be minimized throughout the solution. In principle, this can be achieved by applying any loads sufficiently slowly and smoothly that the kinetic energy in the structure remains negligibly small, but in reality, there are many details that have to be fine tuned to actually achieve this aim. Based on the extensive guidance provided in the LS-DYNA manual (LS-DYNA, 2013), here, we use three ways to control our analysis: loading rate, integration time increment, and numerical damping.

First, the integration time increment should be as large as possible to reduce the number of increments to complete the simulation. However, explicit time integration is stable only if the Courant condition is satisfied as shown in (3.1), essentially, the time step should be limited such that a disturbance (stress wave) cannot travel further than the smallest characteristic element dimension in the mesh.

$$\Delta t \leq f * \left[\frac{h}{c}\right]_{\min} \tag{3.1}$$

where

Δt is the time increment, f is the stability time step factor, h is the characteristic dimension of an element and c is the local material sound speed in an element.

Second, Increase load rates could reduce the time scale of the simulation since fewer increments are needed to complete the job. Usually, it is recommended that the loading rate should be limited to be less than 1% of the wave speed of the material to avoid the collapse of the elements under high frequent collision (Abaqus, 2011). The speed of sound of the material is affected by two properties: the elastic properties and density. The relationship is described in equation (3.2). The wave speed for the colonoscope is around 75m/s. In our work, the insertion velocity of the colonoscope is selected as 60cm/s.

$$c = \sqrt{\frac{K_s}{\rho}} \tag{3.2}$$

Where

K_s is a coefficient of stiffness, the isentropic bulk modulus

ρ is the density.

To ensure the quasi-static properties of the interaction between colon and colonoscope, a numerical contact damping was introduced in the model to dissipate vibration due to high push loading rate of the colonoscope. The amount of numerical damping should be as small as possible to avoid affecting the results of the simulation since the maximum stable time increment will be decreased with the increase of the contact damping (LS-DYNA, 2013). Therefore, in our work, the numerical contact damping coefficient was adjusted to make the time increment for the explicit simulation up to 7e-6s. The Table 3- 3 summarized the mean duration for the insertion simulation of UTC, PDC, and SDC in RSJ, RSF and THF models.

Table 3- 3 Mean duration for the insertion simulation

Colon	RSJ			RSF			THF		
Colonoscope	UTC	PDC	SDC	UTC	PDC	SDC	UTC	PDC	SDC
Computation time (min)	50	78	100	150	240	380	100	180	140

At the same time, for both the colon and colonoscopes, we checked that the ratio of kinetic energy to the internal energy remain lower than 10% for most of time during all simulations, Fig. 3- 6, Fig. 3- 7 and Fig. 3- 8 demonstrates the comparison of kinetic energy and internal energy evolution of the insertion simulation of SDC in RSJ, RSF and THF model, respectively. Fig. 3- 9, Fig. 3- 10 and Fig. 3- 11 illustrates the ratio of kinetic energy to internal energy for colonoscope and colon during insertion simulation in RSJ, RSF and THF model, respectively.

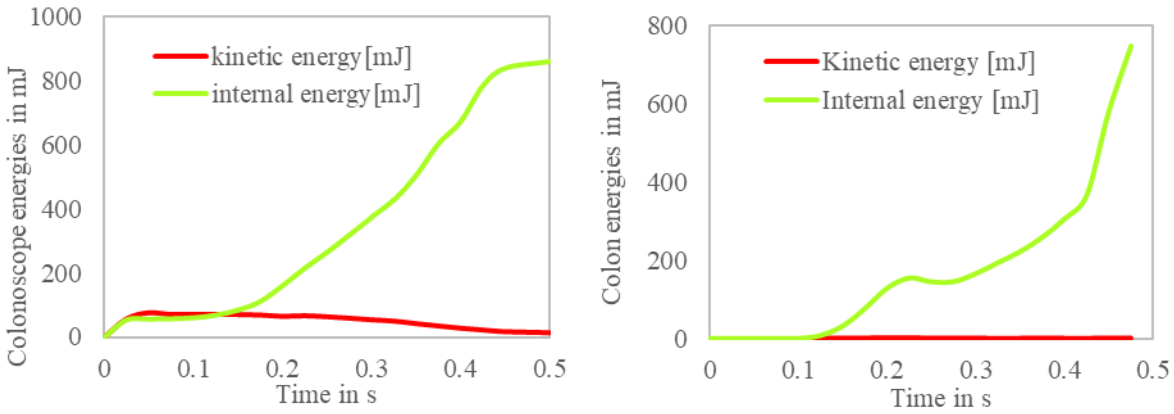

Fig. 3- 6 Average kinetic energy and internal energy evolution for colon and SDC in RSJ model.

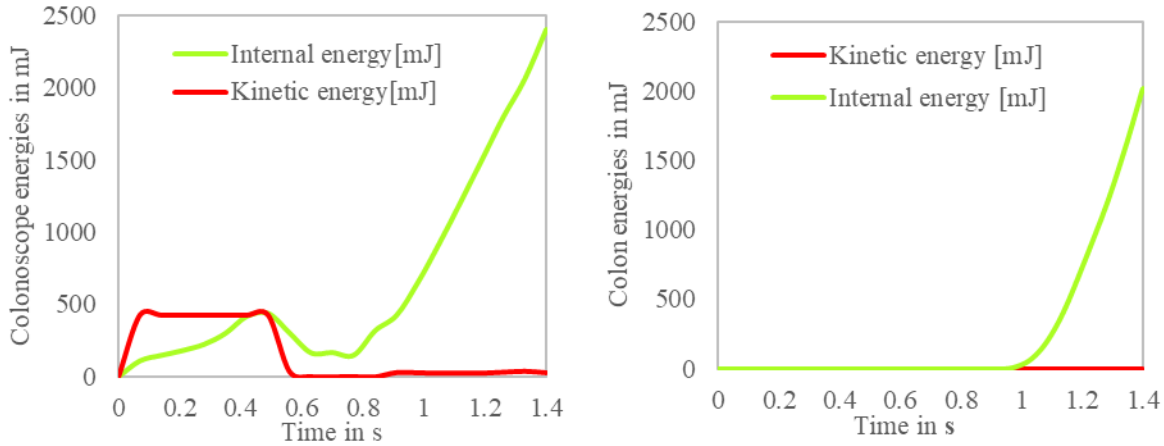

Fig. 3- 7 Average kinetic energy and internal energy evolution for colon and SDC in RSF model.

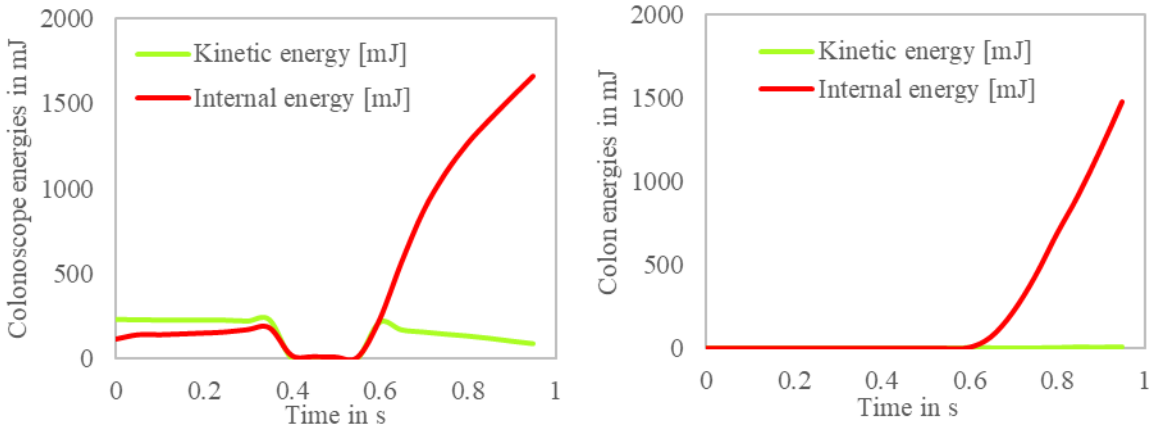

Fig. 3- 8 Average kinetic energy and internal energy evolution for colon and SDC in THF model.

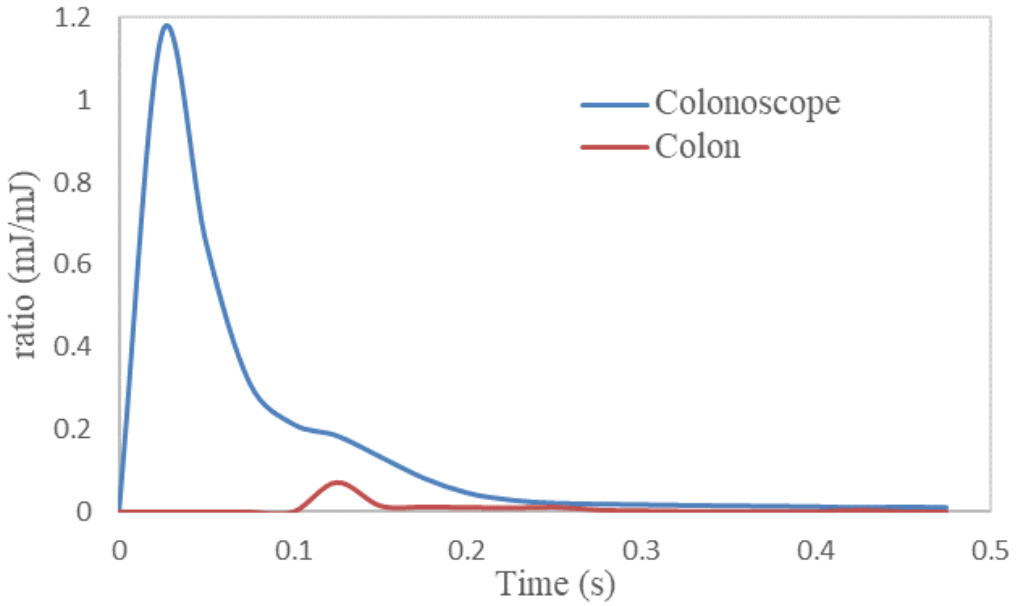

Fig. 3- 9 Ratio of kinetic energy to internal energy for colonoscope and colon in RSJ model

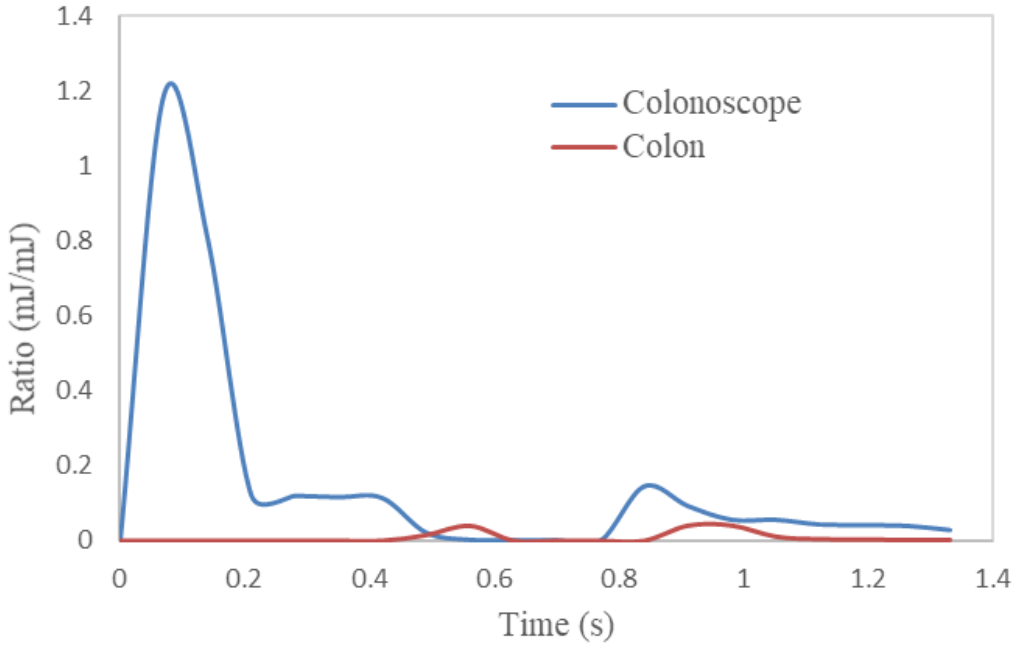

Fig. 3- 10 Ratio of kinetic energy to internal energy for colonoscope and colon in RSF model

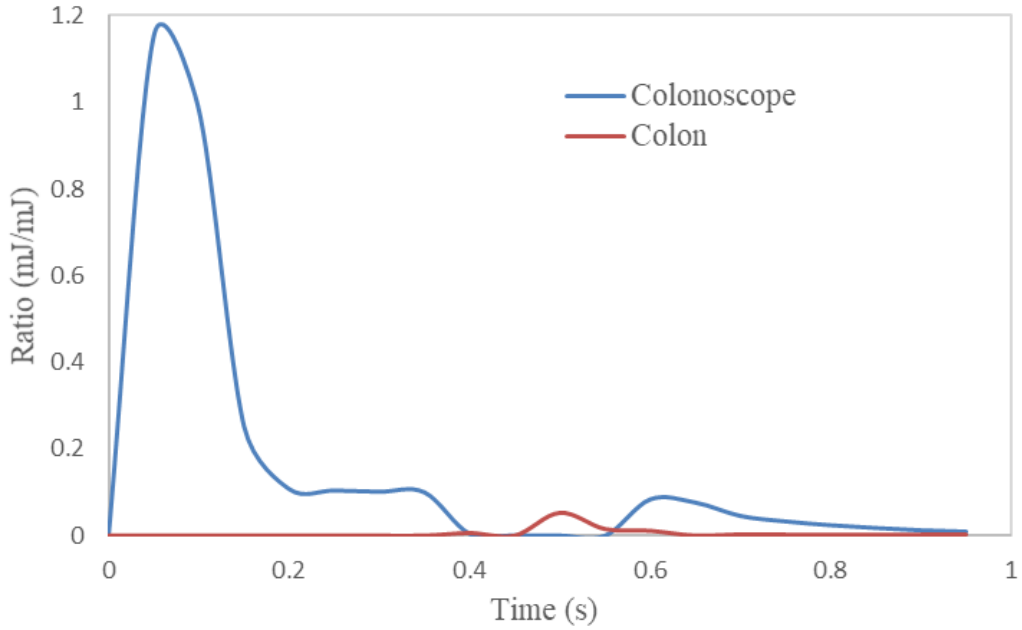

Fig. 3- 11 Ratio of kinetic energy to internal energy for colonoscope and colon in THF model

CHAPTER IV

MATERIAL PARAMETERS OPTIMIZATION

4.1 Introduction

From the mathematical point of view, the mechanical model of colon properties can be fitted easily by using an integral function, and the parameters C_{10}, C_{01} and C_{11} defined in equation (2.22) were generally determined by adopting the trial-and-error or curve fitting method based on the experimental data (J.A. Weiss et al. 2002). However, some conventional curve fitting methods were sometimes not credible due to neglecting the natural property of the soft tissues (Z.W. Wang & C.Y. Tang.2009). Also, it's not accurate to get the unknown parameters through the curve fitting with only tensile test data. (ANSYS, 2009). For those problems an inverse approach is suitable in which a simulation model is used that represents the real geometry, boundary conditions and the sequence of the measurement setup. The unknown parameters are than determined by an iterative approach by comparison between measurement and simulation data. This process is called inverse model calibration (Kunath, S., et al. (2015)). At present, the set of the most widely preferred techniques for the inverse identification of material parameters includes, among other tools, optimization methods based on the training of artificial neural networks (Lehký, D&Novák, D. 2013) Considering commercial computing systems, a very powerful instrument to perform inverse analysis currently appears to consist in the optiSLang program (optiSLang. 2014), which offers a robust

algorithm comprising a broad spectrum of optimization procedures suitable for the inverse identification of material parameters (Most, T. 2010, Hokeš, F. et al. 2016).

In these paper, the parameters C_{10}, C_{01} and C_{11} were identified through an optimization procedure with the use of ANSYS and Optislang programs. Numerical and experimental approaches were performed to realize such an optimization procedure.

4.2 Experimental and Numerical Analysis

4.2.1 Experimental Details

A uniaxial tension test of porcine colon at a quasi-static loading rate of 1cm/min was conducted as shown in Fig. 4- 1 to find the raw load-displacement curve. 8 Specimens from different parts of the porcine colon tissue were prepared. The dimensions of each sample were 10cm in length (length within the grippers) and 2.5cm in width. The mean force-displacement curve was shown in Fig. 4- 2, which shows highly nonlinear relationship.

Fig. 4- 1 (a)Porcine colon. (b) Experimental set-up

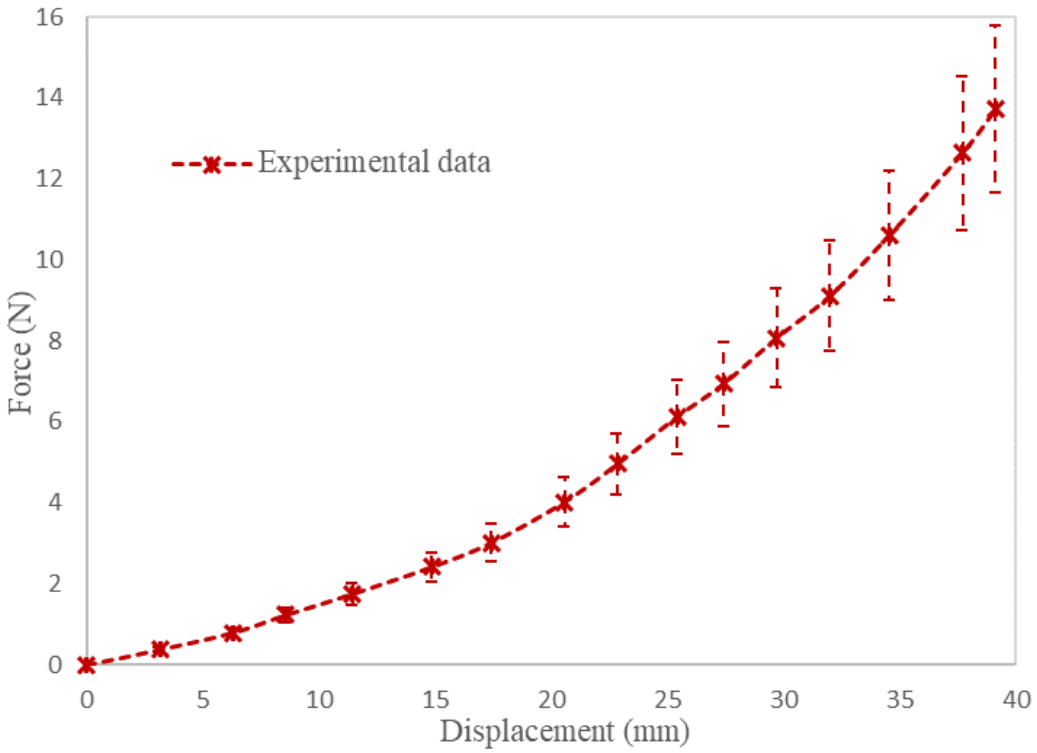

Fig. 4- 2 Mean experimental force–displacement response of porcine colon

4.2.2 Computational Model

As the colon is almost an incompressible hyperelastic material, 4-node shell elements with the capability of modelling this material were used to construct a 3D FE model of the colon specimen as shown in Fig. 4- 3. When displacement load was applied onto the right surface, the total node reaction force F_{simu}^{i} in the left surface can be easily extracted through the signal processing after the FE program was executed. Based on the optimized results, the constitutive material parameters of the colon were inputted into the FE program.

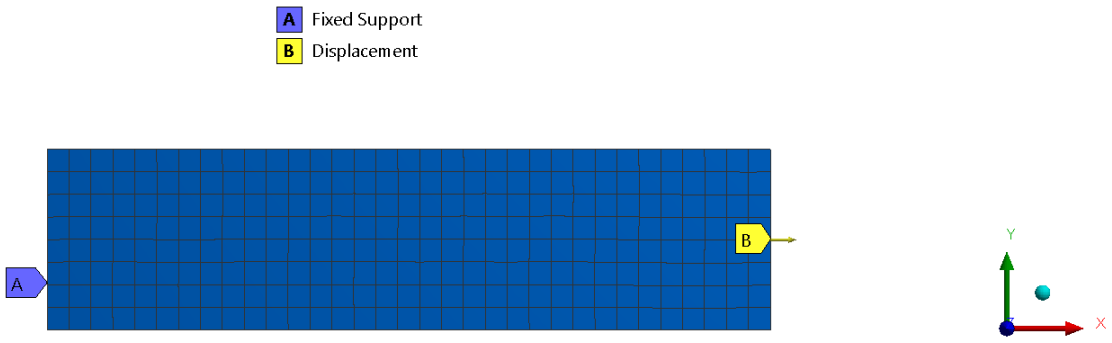

Fig. 4- 3 FE model of the Colon specimen

4.2.3 Optimization Objective Function

Generally, the initial shear modulus (G) is given as

$$G = 2(C_{10} + C_{01}) \tag{4.1}$$

For incompressible materials under infinitesimal strain conditions

$\gamma = 0.5$

$E = 2G(1+\gamma)$

Therefore,

$E = 6(C_{10} + C_{01})$

The initial estimates of hyperelastic coefficients, C_{10} and C_{01}, were determined by setting them equals to each other. From the experiment result, the mean value of young's modulus for porcine colon tissue under strain (10%) is 0.36Mpa and 2.5Mpa under the strain before the fracture of the specimen (60%). therefore, the initial guess for three parameters was given at

$$C_{10} = C_{01} = 0.03Mpa;\ C_{11} = 1.25Mpa$$

The optimization objective function is written as

$$\text{Min}\,(e_1 = \sqrt{\sum_{i=1}^{k}(F_i^{EXP} - F_i^{SIMU})^2}\,) \tag{4.2}$$

s.t C_{10}, $C_{01} \in [0, 0.06Mpa]$, $C_{11} \in [0, 2.5Mpa]$

Where k denotes the number of data samples, F_i^{EXP} is the experimental value of tensile force for the *ith* sample, and F_i^{SIMU} is the simulated data obtained from the ANSYS for the corresponding step, e_1 is the discrepancy between the calculated and the experimental data.

4.3 Optimization Procedures and Results

The optimization process in this work was carried out with the use of ANSYS Optislang software as shown in Fig. 4- 4. As a first step, three material parameters C_{10}, C_{01} and C_{11} were selected as input parameters. The relationship between the reaction force F_i^{SIMU} and displacement load derived from the numerical simulation inside ANSYS was saved in a binary solver file (file.rst). The Signal Processing is available in Optislang in ANSYS, which can read and parameterize the displacements and forces of simulation from the solver file as signal simulation. Meantime, the experimental force-displacement data were also parameterized as signal reference through Signal processing. From Fig. 4-4, noted that both signals did not have the same discretization. To calculate the objective difference between F_i^{EXP} and F_i^{SIMU} from two signals, the abscissa from the Signal Reference was extracted and then interpolated to the abscissa of the Signal simulation. The initial objective difference between the simulation result based on initial guess of

parameters and the reference was calculated. From 0, it was noticed that the initial objective difference was 16.0315.

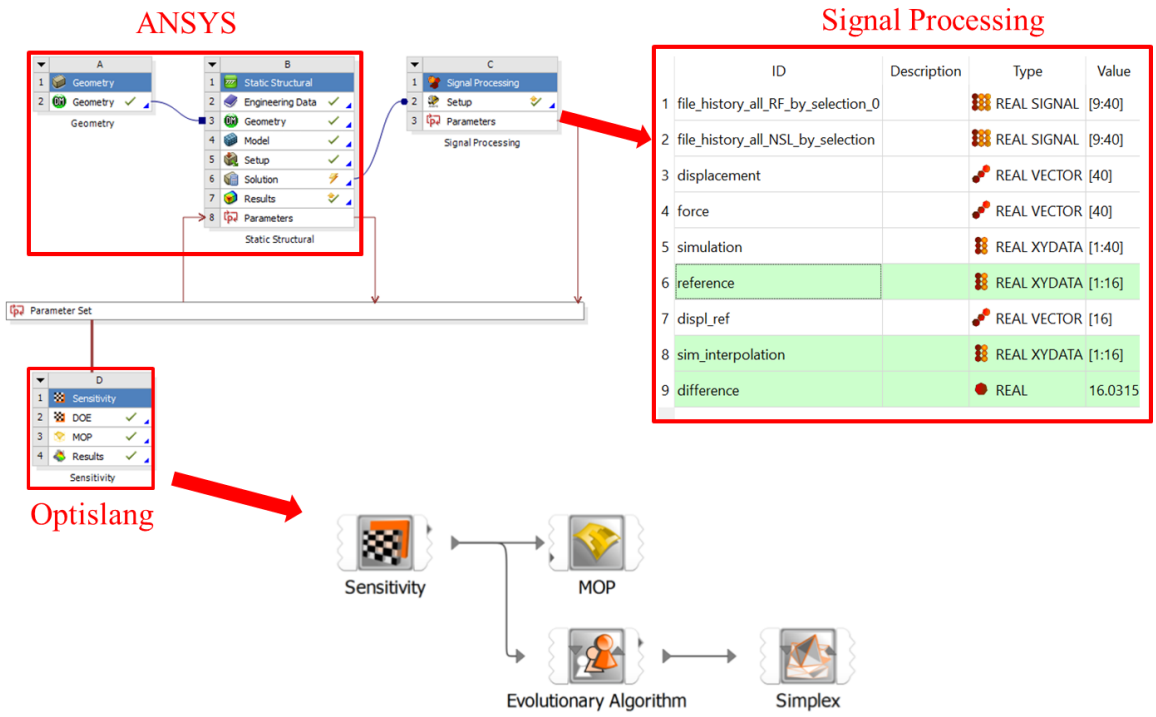

Fig. 4- 4 Optimization process with the use of ANSYS Optislang program

The optimization flow chart proposed by (Kunath, S., et al. (2015) inside Optislang was used in this work. It consists three steps: sensitivity analysis, global optimization using evolutionary algorithm and local optimization using simplex method. At first, all designs achieved through the sensitivity analysis were ranked from low to high in terms of the objective difference e_1, and then top 10 best designs were selected and plotted as shown in Fig. 4- 5. The next step was the conduction of a global optimization using an Evolutionary Algorithm with the 10 best designs of the sensitivity study as a start population. This improves the convergence of the optimization process significantly. As a result, a best design with $e_1 = 1.02$ was achieved. Fig. 4- 6 showed the force-displacement curve of the best design derived from the evolutionary algorithm. The

best design was then used as a start design for a local optimization. For the local search, the Simplex method was used. Fig. 4- 7 showed the evolution of objective difference during the 38 iterations. The final optimized parameters are 652.01 *Pa*, 42.8 *kPa*, and 219.1 *kPa*. for C_{10}, C_{01} and C_{11} with $e_1 = 0.0845$. The optimized result was plotted as a solid line as shown in Fig. 4- 8. It is noticed that there is good agreement between the simulated and experimental hyperelastic behaviour of the colon as represented by their force–displacement relations. Thus, it verified that the proposed optimization scheme for the parameters of Mooney–Rivlin model was reliable.

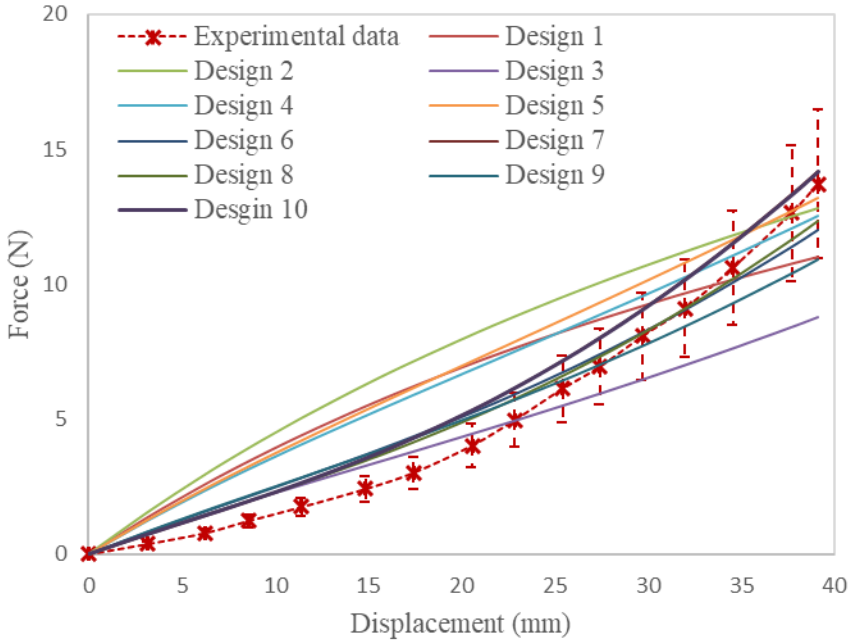

Fig. 4- 5 Top 10 best designs from sensitivity analysis

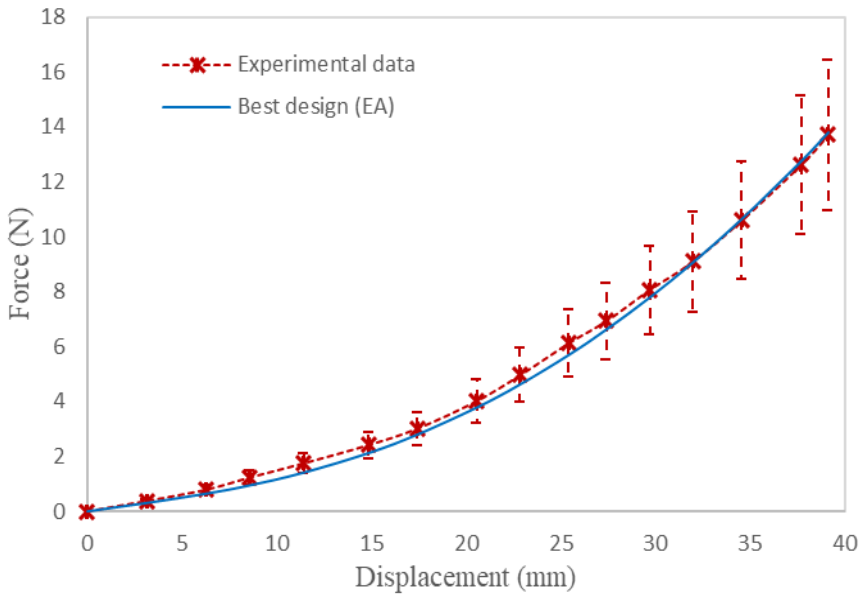

Fig. 4- 6 Best design from global optimization using an Evolutionary Algorithm

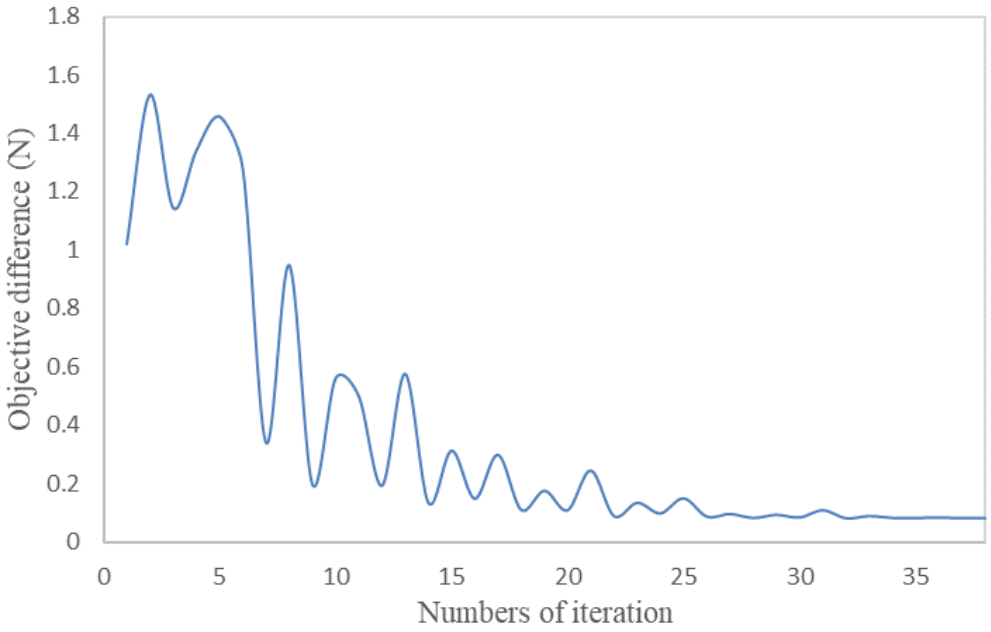

Fig. 4- 7 Evolution of objective difference along with the iteration

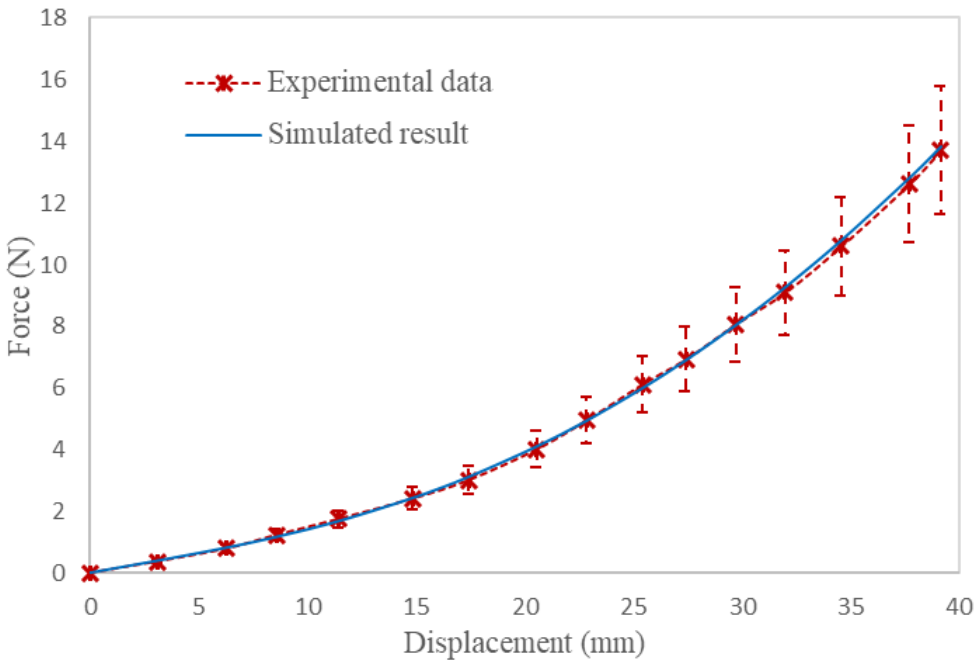

Fig. 4- 8 Optimized design from local optimization using simplex method

CHAPTER V

SIMULATION RESULTS

Based on the summary about the anatomic differences of the human colon in terms of age, region, and gender, the aged patients tend to have more fixed sigmoid angulation as well as higher contact friction during the interaction between colon and colonoscope during colonoscopy. One of the main structural differences for human colon in terms of region is internal colon diameter. Females tend to longer and deeper transverse colons and lower fixation of sigmoid-descending junction. Therefore, in our work, the effects of age and region on the efficiency of SC colonoscopes in reducing patient pain compared with that of SDC were predicted by comparing the colon deformation in RSJ model. As for the influence of gender, it was predicted by comparing the colon deformation in RSF and THF models.

5.1 Influence of Age

The influence of age on the efficacy of SC colonoscopes was predicted from two aspects: 1) Colon deformation induced by UTC, PDC, and SDC when negotiating the fixed recto-sigmoid junction; 2) The influence of contact friction coefficient on the behavior of UTC, PDC, and SDC in terms of colon deformation

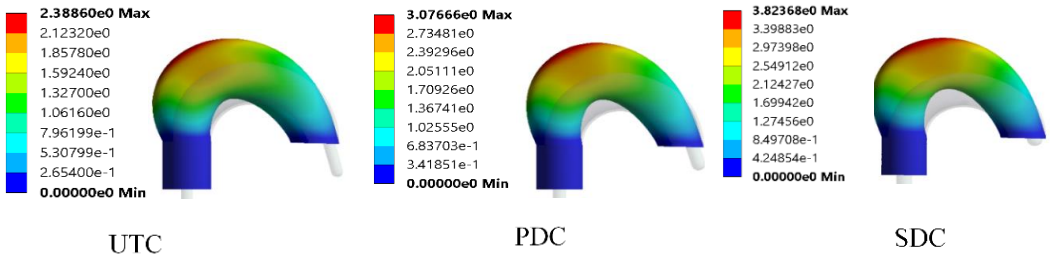

Fig. 5- 1 Final colon deformation(cm) in RSJ (D=36 mm)

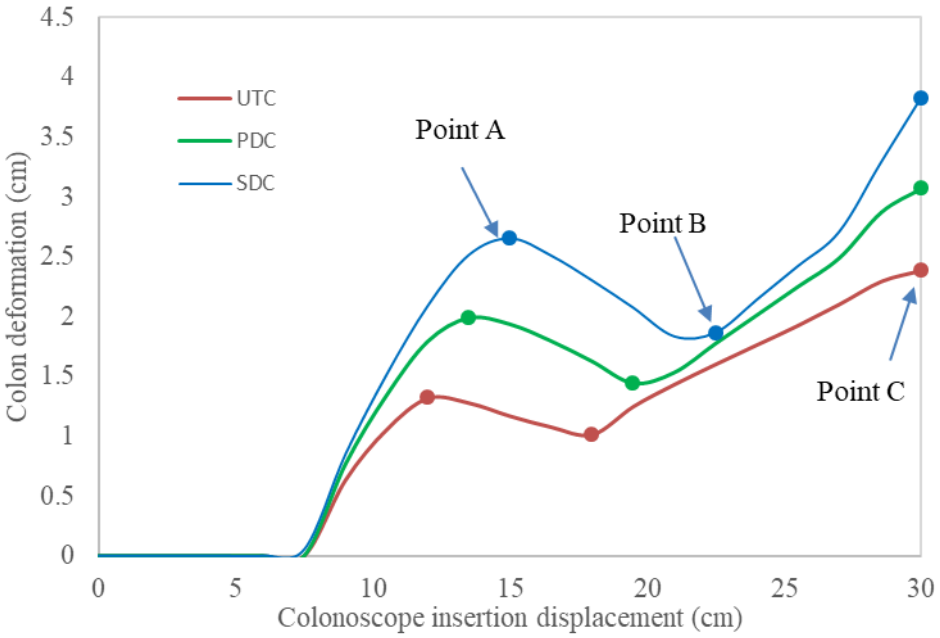

Fig. 5- 2 Colon deformation in RSJ (D=36 mm)

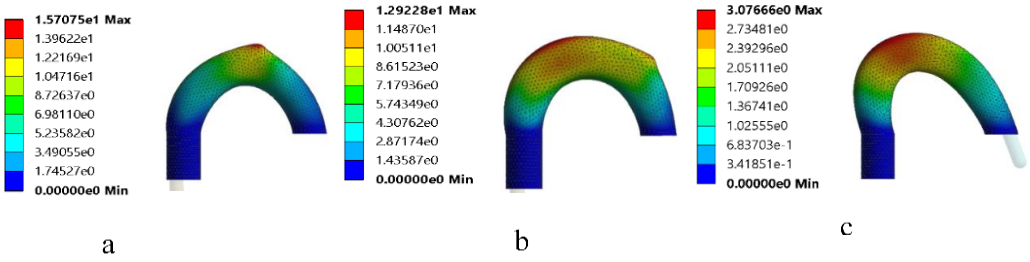

Fig. 5- 3 Three positions (a, b and c) of PDC in RSJ (D=36 mm)

Fig. 5- 1 and Fig. 5- 3 shows the final recto-sigmoid colon deformation and plots due to the insertion of UTC, PDC and SDC, respectively. It was noticed that SDC caused the maximum final colon deformation (3.82cm) compared to PDC (3.07cm) and UTC(2.39cm) when negotiating the fixed recto-sigmoid junction from Fig. 5- 1. It was also noticed that all curves show same trend and three special points existed in all curves as marked in Fig. 5- 2: point A, point B, and point C. Fig. 5- 3 shows three positions during the insertion process of a PDC in RSJ model: point a, point b, and point c. The insertion time of these three points corresponds to point A, point B, and point C in Fig. 5- 3, respectively. Therefore, the following three aspects could be obtained: 1) point A corresponds to the maximum colon deformation when a colonosocpe negotiates the acute angulation of sigmoid colon; 2) point C corresponds to the maximum colon deformation when the colonoscope passes through the fixed constraining; 3) colon deformation at point C is always larger than that at point A.

Based on the above analysis, for older patients, an SC colonoscope causes lower overall and maximum patient pain compared with SDC.

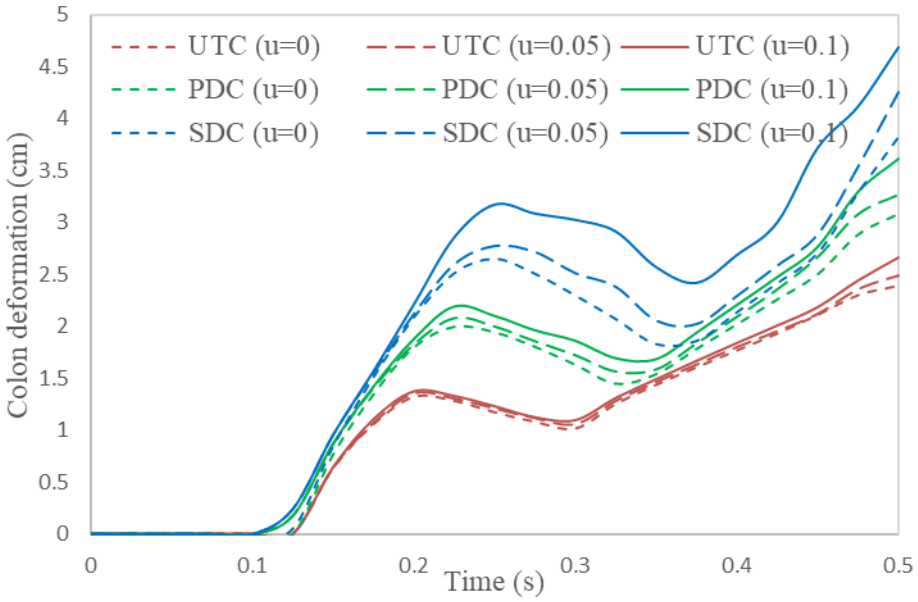

Fig. 5- 4 Colon deformation under different contact friction coefficients in RSJ

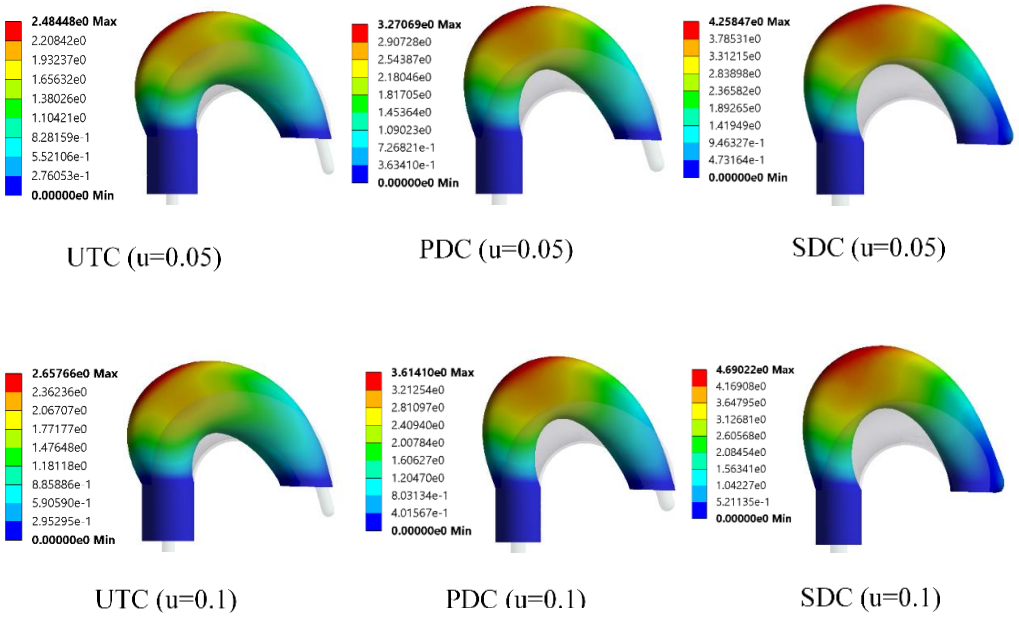

Fig. 5- 5 Final colon deformation for different contact friction coefficient (u=0.05, 0.1)

As for the influence of contact friction coefficients on the performance of colonoscopes, three different contact friction coefficients (u), including 0, 0.05, and 0.1 were selected and applied to the insertion simulation for UTC, PDC and SDC in RSF model. Fig. 5- 1, Fig. 5- 5 and Fig. 5- 4 shows the final colon deformation for u=0, u=0.05 and 0.l, and plots for all three contact friction coefficients. It was noticed that SC colonoscopes (UTC and PDC) caused less colon deformation (overall and maximum) compared with SDC under the same contact friction coefficient. At the same time, UTC and PDC were less sensitive to the increase of the contact friction than SDC in terms of the increase of colon deformation.

Therefore, it could be predicted that SC colonoscopes are more effective in reducing patient pain for older patients compared with that of SDC since older patients tend to have more fixed angulations of the sigmoid colon as well as higher friction colons.

5.2 Influence of region

To account for regional difference, two different internal colon diameters (D), including 3.6cm for African patients, and 2.3cm for European patients were selected. Fig. 5- 6 and Fig. 5- 7shows final colon deformation and plots induced by UTC, PDC and SDC in RSJ (D=2.3 cm). Table 5- 1 and Table 5- 2summarizes colon deformation and relative differences with respect to SDC at point A and point C, respectively. Note that, compared with SDC, SC colonoscopes reduce more colon deformation at point A and C for RSJ model with D=2.3 cm than that with D=3.6 cm.

Therefore, it could be predicted that compared with African patients, small-caliber (SC) colonoscopes are more helpful in reducing patient pain for European patients due to smaller diameter colons.

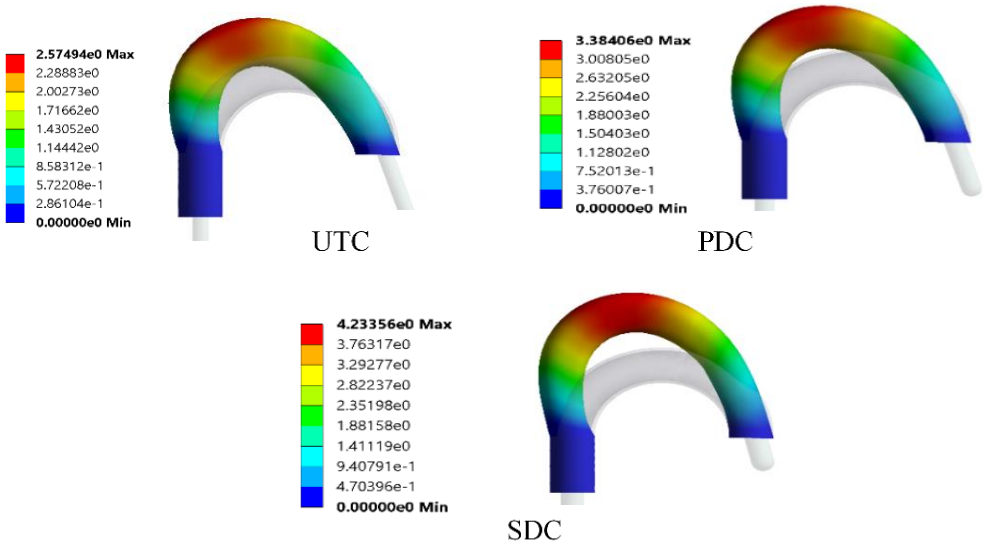

Fig. 5- 6 Colon deformation induced by UTC, PDC and SDC in RSJ (D=23 mm)

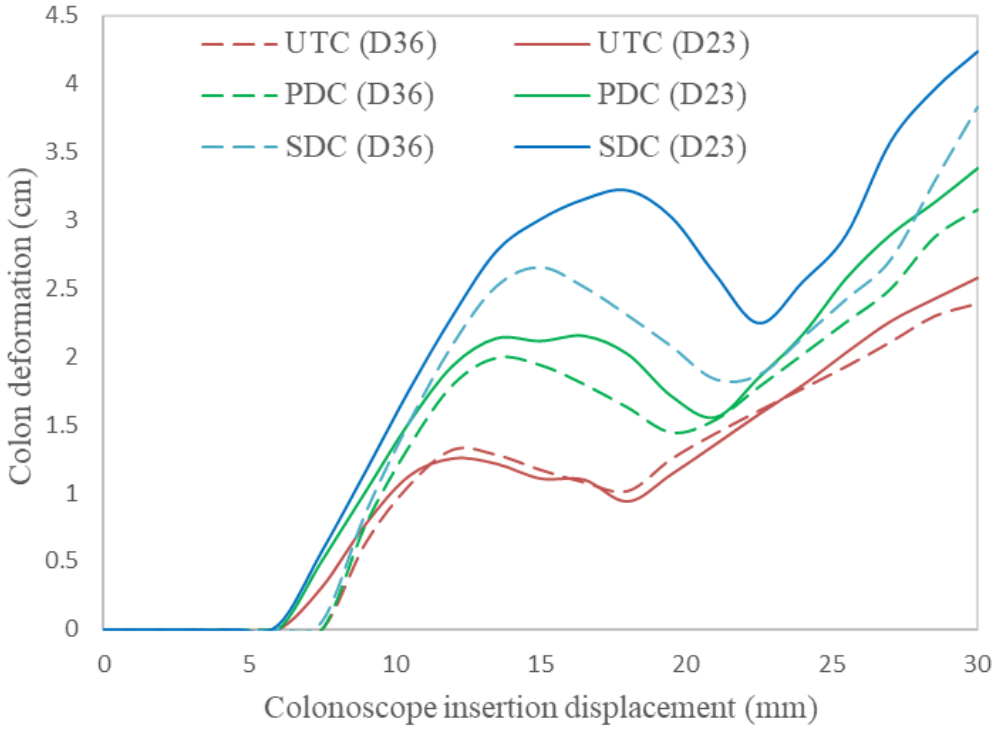

Fig. 5- 7 Deformation of colon (D=23mm and D=36mm) induced by UTC, PDC and SDC

Table 5- 1 Colon deformation and relative difference at point A

	UTC		PDC		SDC	
Colon internal diameter (mm)	23	36	23	36	23	36
Colon deformation at point A (cm)						
	1.353	1.319	2.155	1.992	3.218	2.651
Difference with respect to SDC (cm)						
	-1.865	-1.332	-1.063	-0.659	-	-

Table 5- 2 Colon deformation and relative difference at point C

	UTC		PDC		SDC	
Colon internal diameter (mm)	23	36	23	36	23	36
Colon deformation at point C (cm)						
	2.575	2.389	3.384	3.077	4.234	3.824
Difference with respect to UTC (cm)						
	-1.659	-1.435	-0.85	-0.747	-	-

5.3 Influence of Gender

5.3.1 Simulation results of RSF model

One of main differences between the female and the male colon is that the deeper pelvis of women causes a lower location of the sigmoid-descending junction. In our study, such difference was simplified as the change of angle α as marked in Fig. 3- 2. Three different angles 0°, 30° and 45° were selected and simulated. Fig. 5- 8 shows the final colon deformation induced by an UTC, a PDC and a SDC during the insertion simulation inside RSF model. Table 5- 3 summarized differences of final sigmoid colon deformation induced by SC colonoscopes with respect to that induced by SDC for RSF model. It was notice that: compared with the colon deformation induced by SDC, for α= 0°, UTC and PDC caused 1.32 cm and 0.98 cm more colon deformation, respectively; for α= 30°, UTC and PDC reduced 1.75 cm and 0.38 cm colon deformation, respectively; for α= 45°, UTC and PDC reduced 5.048 cm and 1.71cm colon deformation, respectively. The plots of the sigmoid colon deformation during whole insertion simulation for RSF

model when α is 0°, 30° and 45° as shown in **Error! Reference source not found.**, **Error! Reference source not found.** and **Error! Reference source not found.**, respectively.

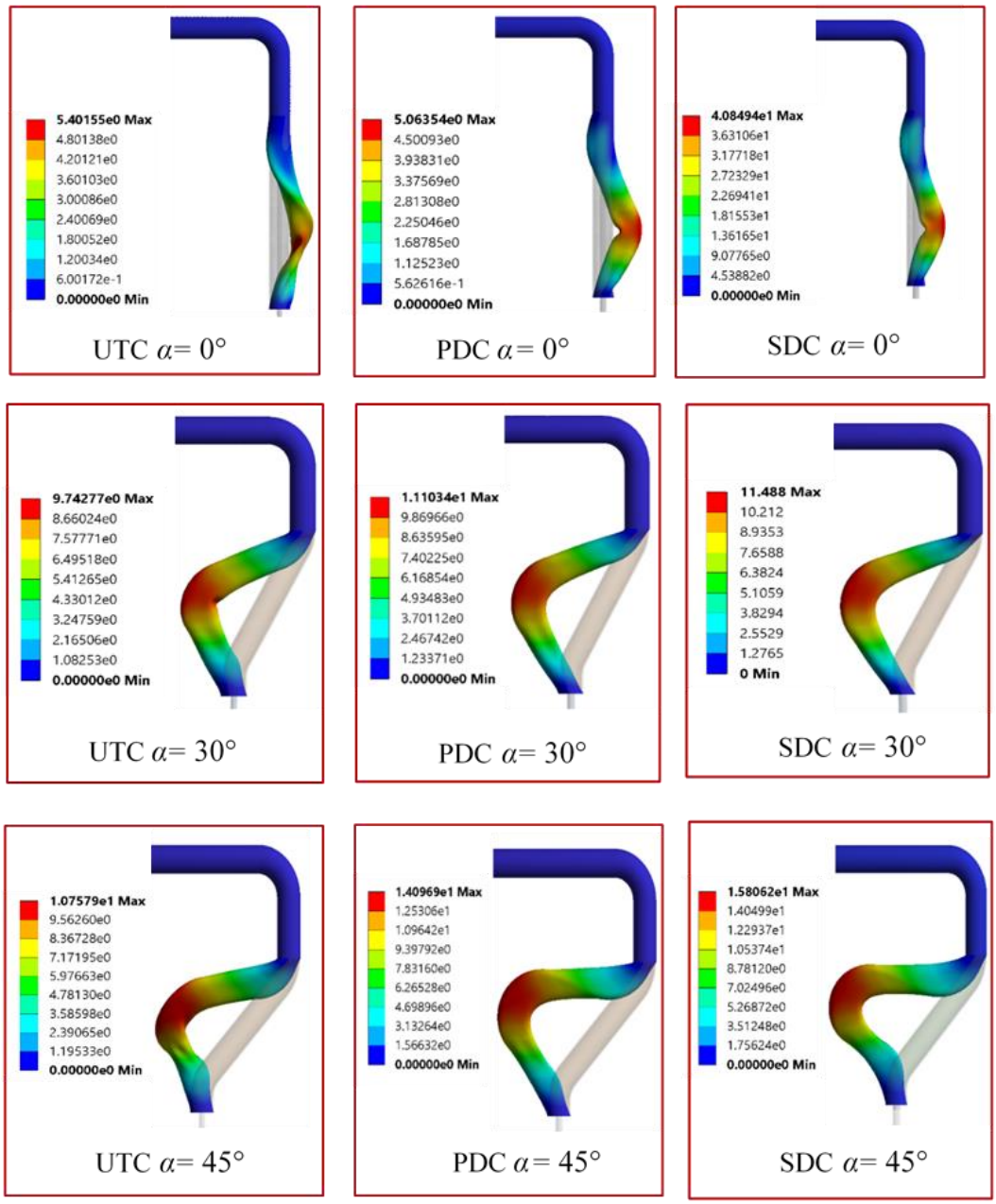

Fig. 5- 8 Final sigmoid colon deformation in RSF model

Table 5- 3 Differences of final sigmoid colon deformation induced by SC colonoscopes with respect to that induced by SDC for RSF model

	Differences with respect to SDC (cm)	
Angle α	UTC	PDC
0 deg	1.32	0.98
30 deg	-1.75	-0.38
45 deg	-5.048	-1.71

By setting the same scale for the y-axis that represents the sigmoid colon deformation in Fig. 5- 9, Fig. 5- 10 and Fig. 5- 11, the influence of angle α on the performance of UTC, PDC and SDC in terms of colon deformation could be compared.

For α= 0°, SC colonoscopes (UTC and PDC) cause slightly more colon deformation during whole insertion simulation. For α= 30°, PDC and SDC show almost the same colon deformation and are larger than that of the UTC. For α=45°, SDC shows much more colon deformation than SC colonoscopes. Meanwhile, it can be observed that the difference of the sigmoid colon deformation induced between SC colonoscopes and SDC show positive correlation with angle α. In addition, it was noticed that the final colon deformation represents the maximum colon deformation, and thus the maximum patient pain could be predicted by comparing the final colon deformation.

In summary, it could be predicted that: (1) the position of fixation of the sigmoid-descending junction has influence on the performance of SC colonoscopes in reducing patient pain. (2) SC colonoscopes are more effective in reducing both overall and

maximum patient pain for patients with lower fixation of the sigmoid-descending junction.

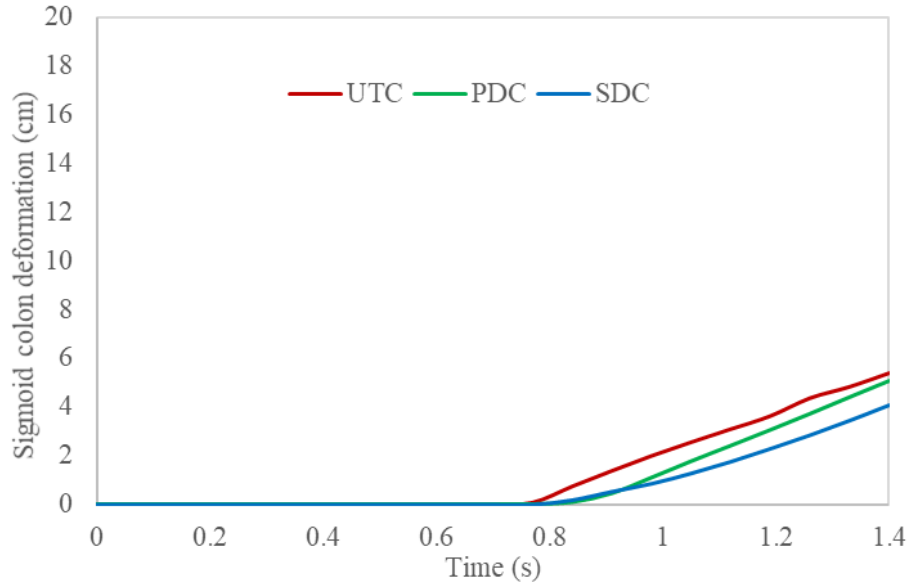

Fig. 5- 9 Sigmoid colon deformation in RSF model ($\alpha = 0°$)

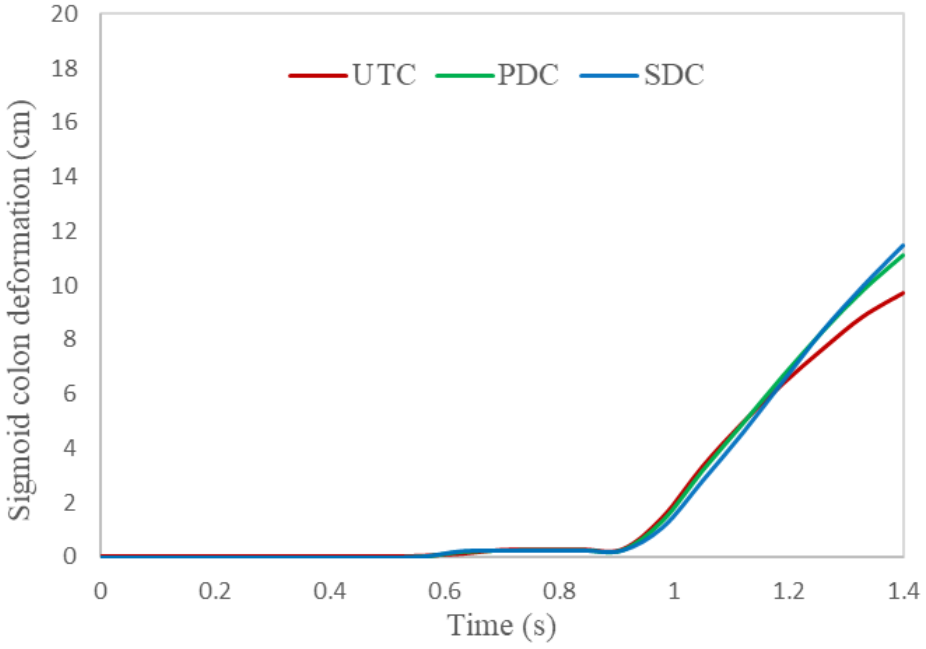

Fig. 5- 10 Sigmoid colon deformation in RSF model ($\alpha = 30°$)

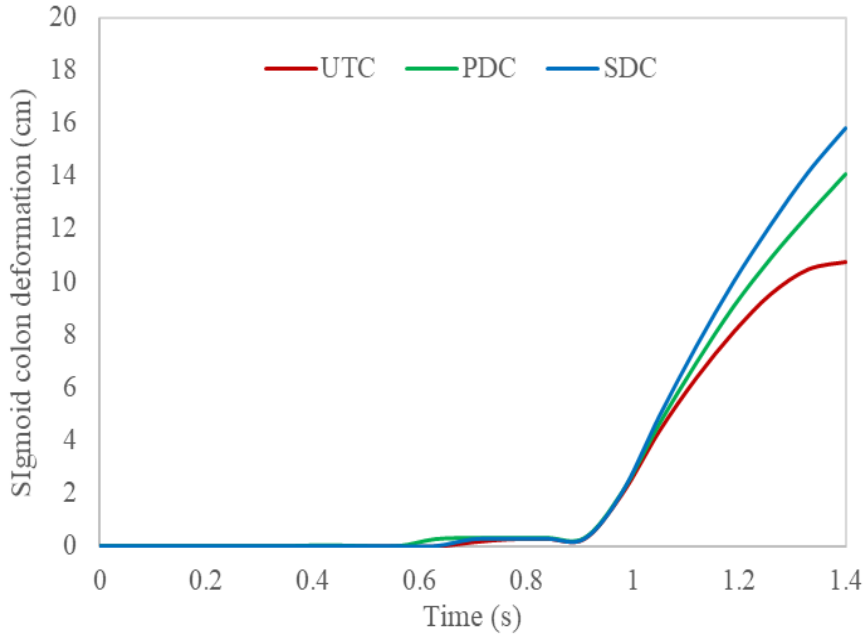

Fig. 5- 11 Sigmoid colon deformation in RSF model (α= 45°)

5.3.2 Simulation results of THF model

One of another difference between the female and the male colons is the length and curvature of the transverse colon. Women tend to have a longer and deeper transverse colon. Therefore, in our study, an angle β as shown in Fig. 3- 3 was introduced to represent the change of the length and curvature of the transverse colon. The insertion simulation for UTC, PDC and SDC in THF model with β=0°, 30° and 45° were simulated. The final transverse colon deformation is shown in Fig. 5- 12 while Fig. 5- 13, Fig. 5- 14 and Fig. 5- 15 demonstrates the plots for transverse colon deformation during insertion simulation in THF model with β=0°, 30° and 45°, respectively. Table 5- 4 summarized differences of final transverse colon deformation induced by SC colonoscopes with respect to that induced by SDC for THF model.

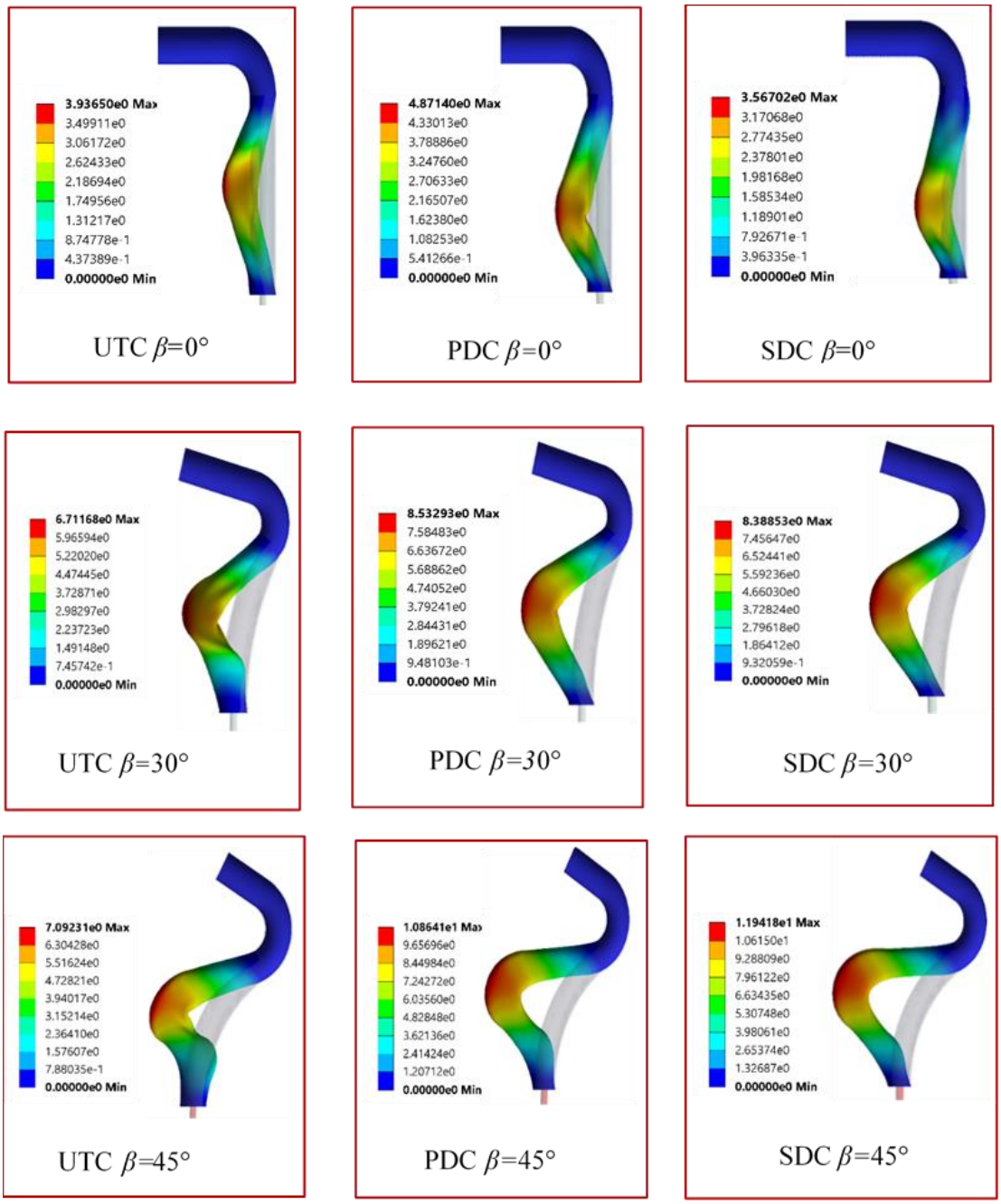

Fig. 5- 12 Final transverse colon deformation for THF model

Table 5- 4 Differences of final transverse colon deformation induced by SC colonoscopes with respect to that induced by SDC for THF model

	Difference with respect to SDC (cm)	
Angle β	UTC	PDC
0 deg	0.37	1.30
30 deg	-1.67	0.12
45 deg	-4.85	-1.08

Simulation results of THF model were similar with that of RSF model. For β=0°, UTC and PDC caused 0.37cm and 1.3cm more final transverse colon deformation than that caused by SDC. For β=30°, PDC and SDC showed almost the same transverse colon deformation during most of the simulation time after the scope began to buckle, which are greater than UTC. For β=45°, SDC shows the maximum colon deformation and the reduction of final transverse colon deformation were 4.85 cm for UTC and 1.08 cm for PDC. Therefore, it can be predicted that: (1) the length and curvature of the transverse colon have influence on the performance of SC colonoscopes in reducing patient pain. (2) SC colonoscopes are more effective in reducing both patient pain for patients with longer and deeper transverse colons.

In summary, the simulation results of RSF and THF models could be used to further predict the influence of gender of patients on performance efficiency of SC colonoscopes in reducing patient pain, i.e., SC colonoscopes (UTC and PDC) have no advantage in reducing patient pain for men (RSF model with small α and THF model

with small β) while they are more helpful in reducing discomfort for female patients (RSF model with larger α and THF model with larger β).

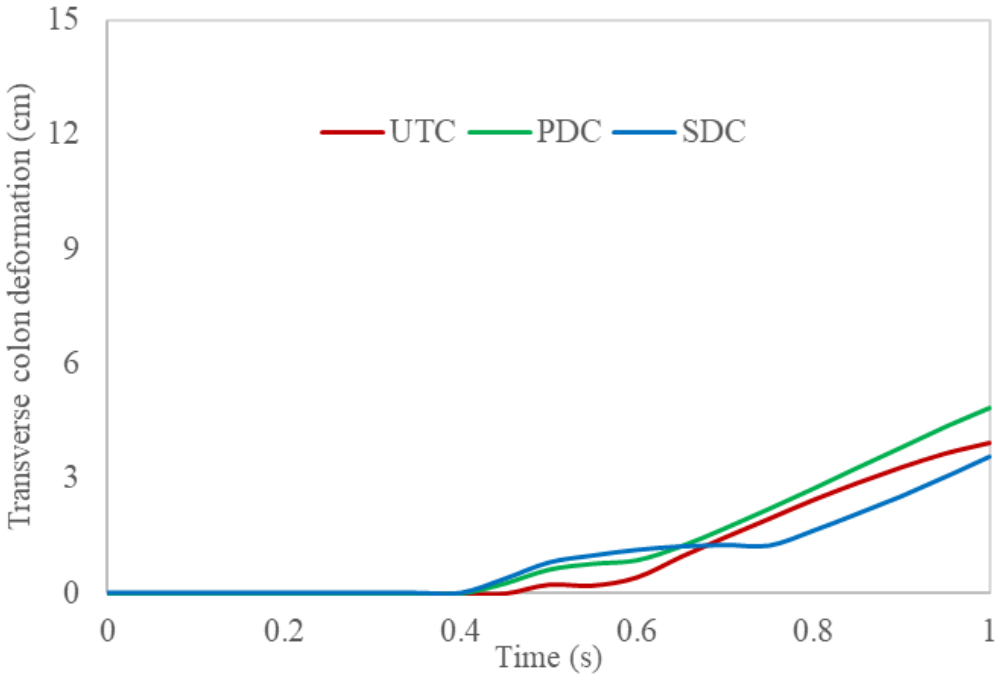

Fig. 5- 13 Transverse colon deformation in THF model (β=0°)

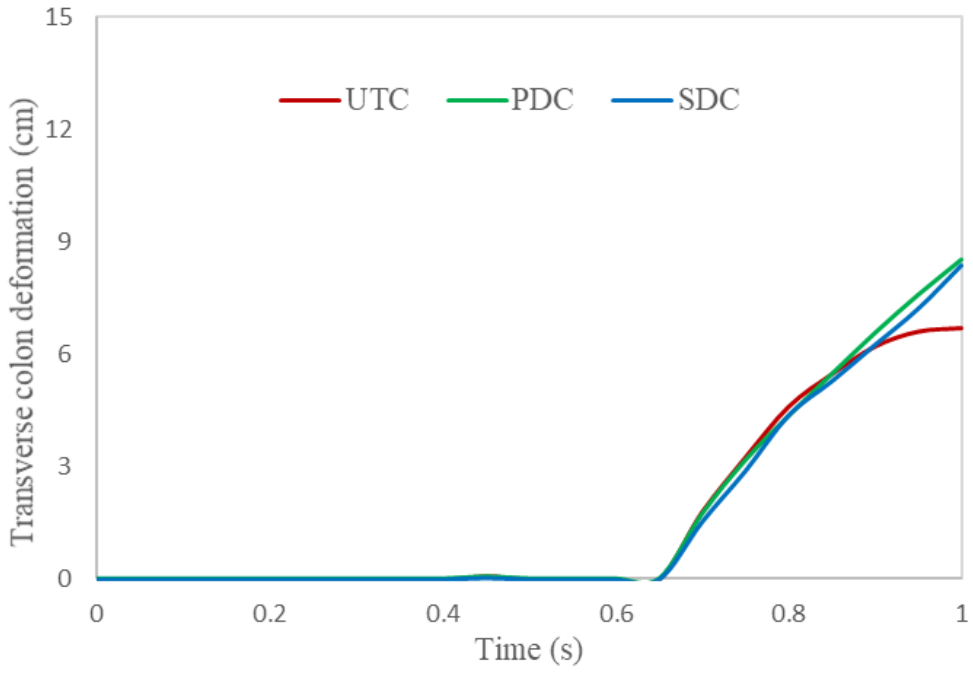

Fig. 5- 14 Transverse colon deformation in THF model (β=30°)

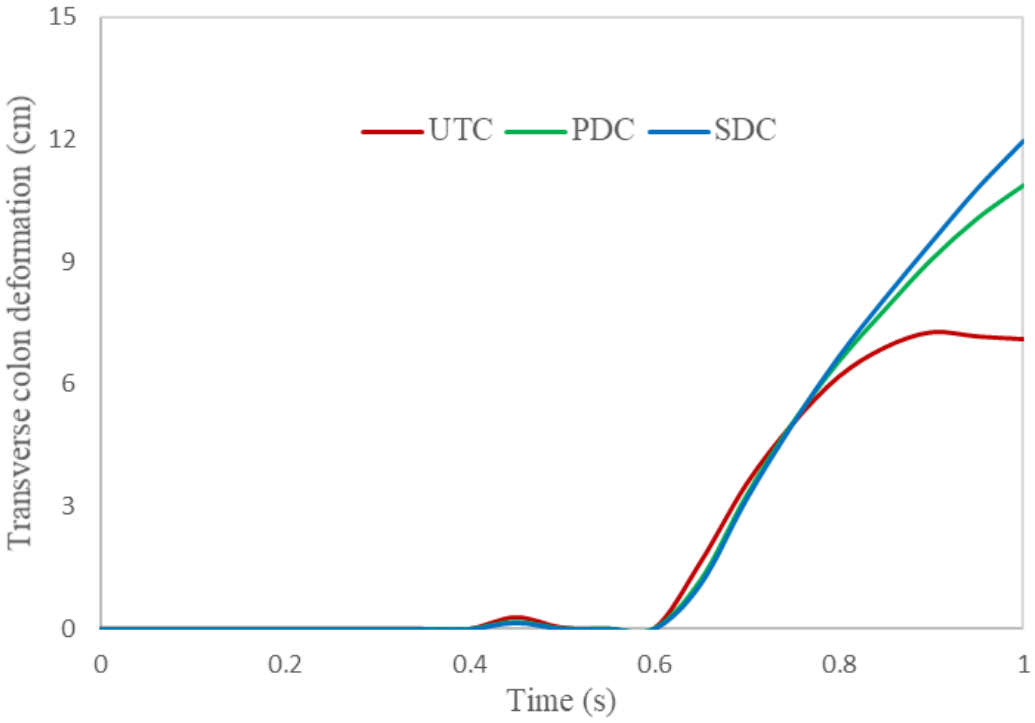

Fig. 5- 15 Transverse colon deformation in THF model (β=45°)

5.4 Simulation results of fixed THF model

The simulation results of RSF and THF models validated the efficacy of SC colonoscopes in reducing patient pain for female patients since they cause less colon deformation when negotiating the splenic and hepatic flexure in RSF and THF models with larger angles compared with the SDC. However, it is known that the SC colonoscope have an easier buckling shaft than the SDC due to the smaller diameter, which may in turn limit the advancement of the colonoscope and causes more colon deformation. Therefore, a contact model between the buckled colonoscope and the colon is needed to provide reasonable insight for the simulation results inside RSF and THF models.

Cheng, W. B., et al. (2012) proposed the insight for the interaction between the colonoscope and colon based on the behavior of oil-well drilling strings used in the petroleum industry. It was stated that drill strings are often in compression and have the tendency to buckle inside the well if the compressive load exceeds the critical threshold and colonoscope has the same tendency to be buckled when negotiating the splenic and hepatic flexure. Also, many studies have been conducted to form the mathematical contact model between the post-buckled drill string and the rigid well (Hajianmaleki, & Daily. (2014), Gao, D., & Huang, W. (2015), Huang, Gao, & Wei. (2015)) and it was found that both the buckled length of the drill string and contact force between drill string and wellbore could affect the drilling performance. Based on this finding, two quantities, including the buckled length of the colonoscope and the contact force between the buckled scope and the colonic wall may have effect on the deformation of colon and should be investigated. However, unlike the buckling process of the drill string whose tip is relatively fixed, the tip of the colonoscope is flexible and keeping passing through the splenic and hepatic flexure. Also, the shapes of the oil-well are quite simple, including a horizontal, an inclined or a curved with constant curvature. Above two aspects make it difficult to derive the mathematical contact model between colonoscope and colon for the RSF or THF model from available drill sting -oil well contact models.

Therefore, in this work, a numerical model which simulated the insertion process of colonoscopes in the fixed THF model was developed, the buckling behaviors of UTC, PDC and SDC and the contact force between the colonoscope and transverse colon segment were studied during the whole insertion simulation.

Fig. 5- 16 shows the final buckling shape of UTC, PDC and SDC due to the insertion in fixed THF model with β=0°, 30° and 45°. Since it is difficult to directly measure the buckled length of colonoscopes within the colon model, distal end displacements of colonoscopes were selected and investigated to further provide insight on the buckled length. It was clearly noticed that, for the insertion simulation in fixed THF model with β=0°, the distal end displacement of UTC is smaller than that for PDC and SDC due to easier buckling shaft. As result, it inferred that the buckled length of UTC was longer than that of PDC and SDC. However, for the insertion simulation in fixed THF model with β= 30° and 45°. The difference in terms of the distal end displacement is not obvious and thus it is difficult to predict the buckled length. Therefore, distal end displacements of colonoscopes in fixed THF model with β=0°, 30° and 45° during insertion simulation were extracted and shown in Fig. 5- 17, Fig. 5- 18 and Fig. 5- 19, respectively. it was noticed that, in comparison to the buckled length of the SDC, SC colonoscopes tended to have longer buckled length. However, the discrepancy of the buckled length between SC colonoscopes and SDC decreased with the increase of angle β.

The contact force during the insertion simulation in fixed THF model with β=0°, 30° and 45° were plotted and shown in Fig. 5- 20, Fig. 5- 21 and Fig. 5- 22, respectively. Noted that the contact force induced by the buckled SC colonoscopes (UTC and PDC) are always less than that induced by the SDC. Also, the discrepancies of the contact force caused between SC colonoscopes and SDC increased with the increase of the angle β.

Both the contact force and buckled length of the colonoscope can contribute to the deformation of the colon. However, based on simulation results in fixed THF model,

these two quantities for SC colonoscopes showed reverse change with the increase of angle β. Therefore, the combined effects of buckled length and contact force may account for the simulation results in RSF and THF models.

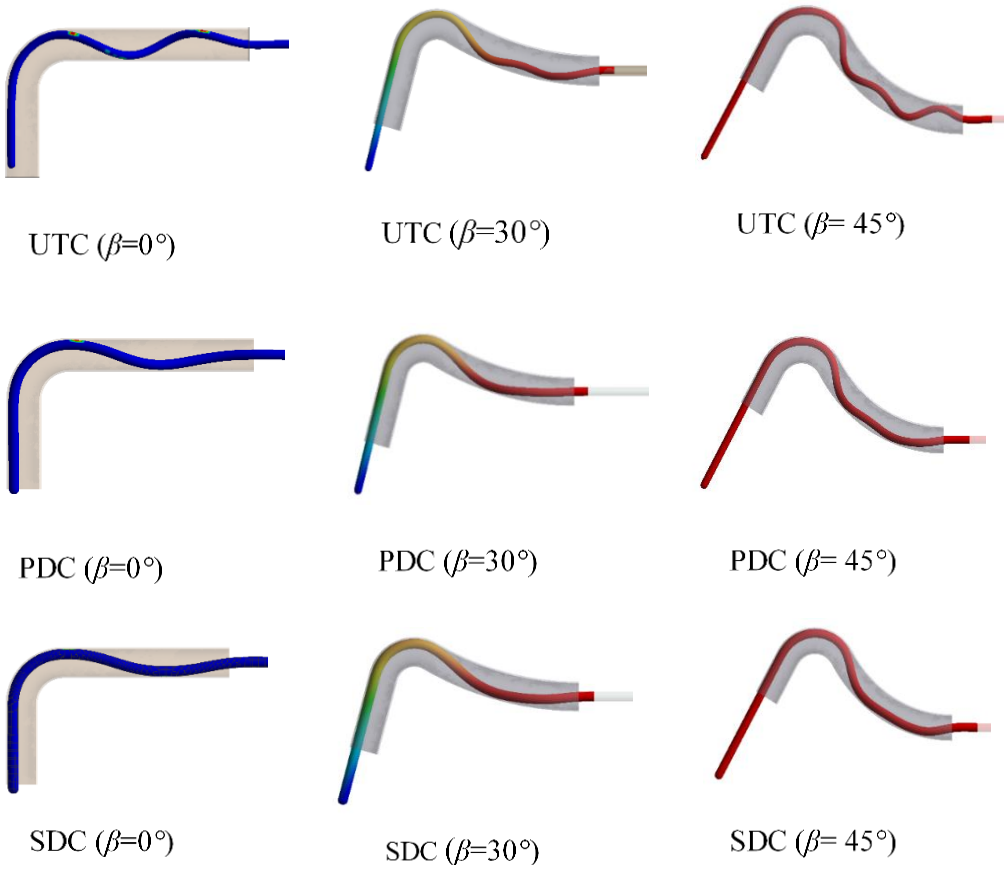

Fig. 5- 16 Colonoscope buckling shape for fixed THF model

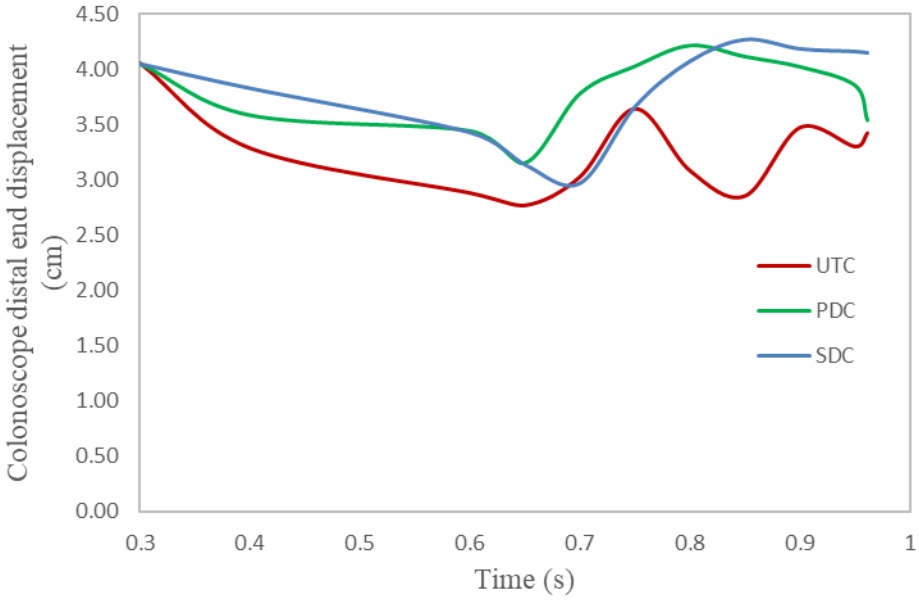

Fig. 5- 17 Colonoscope distal end displacement in fixed THF model (β= 0°)

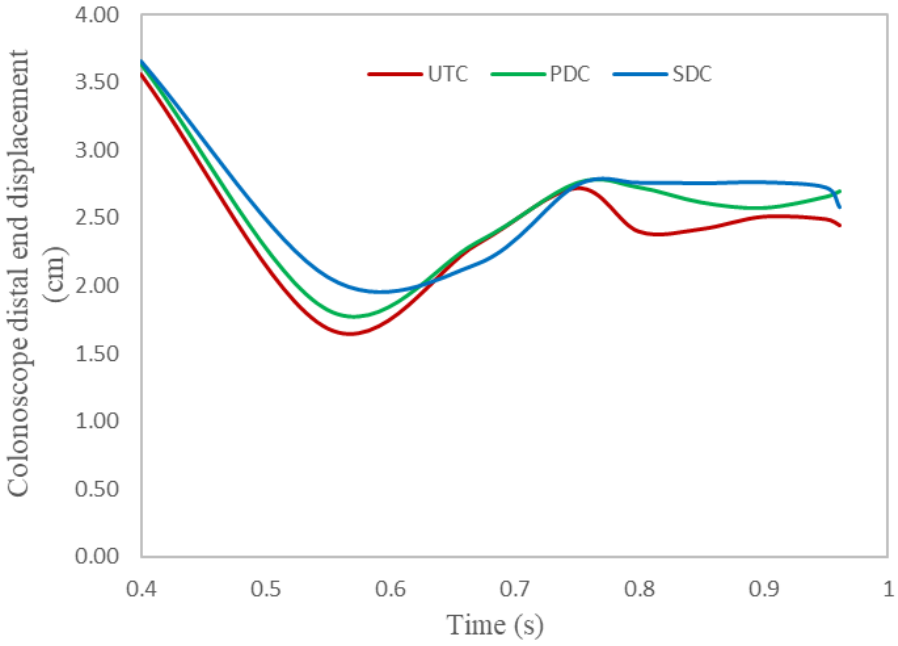

Fig. 5- 18 Colonoscope distal end displacement in fixed THF model (β= 30°)

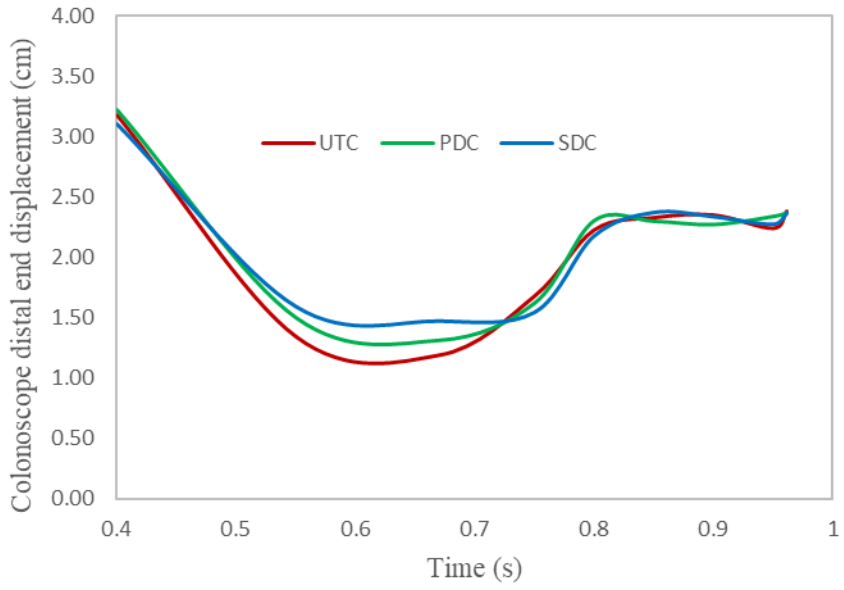

Fig. 5- 19 Colonoscope distal end displacement in fixed THF model (β= 45°)

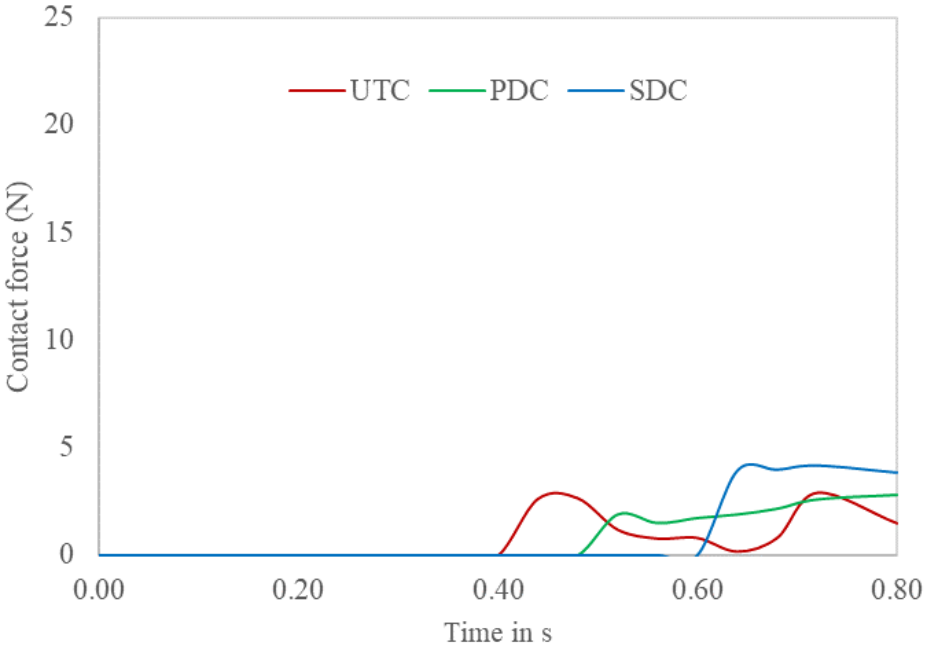

Fig. 5- 20 Contact force in fixed THF model (β=0°)

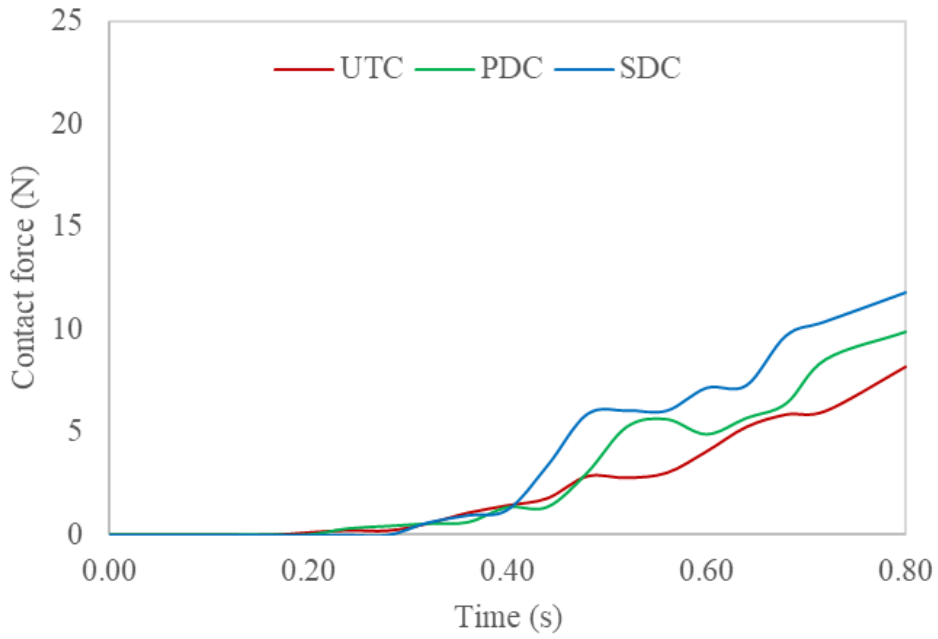

Fig. 5- 21 Contact force in fixed THF model (β= 30°)

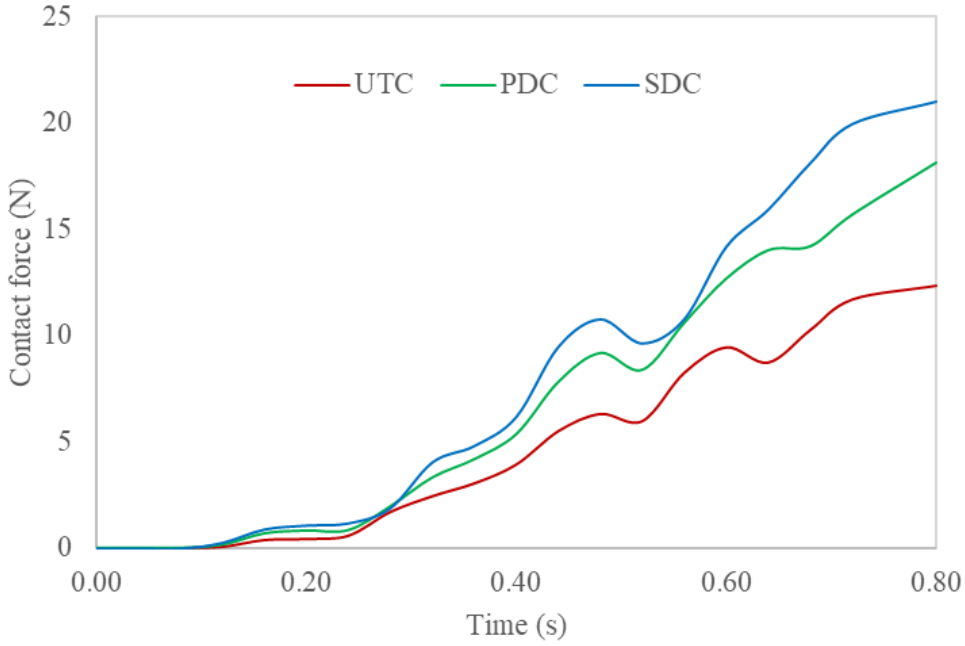

Fig. 5- 22 Contact force in fixed THF model (β= 45°)

CHAPTER VI

CONCLUSIONS AND FUTURE WORK

6.1 Conclusions

In this study, the insertion simulation of colonoscopes with different diameters in colon models considering the effects of gender, age and region of patients was successfully conducted with explicit FEM. A uniaxial tensile test was conducted to provide the experimental data of a porcine colon. Then the parameters of the constitutive material model of the colonic tissue were identified through an optimization procedure.

Before doing the insertion simulation, the anatomical differences for human colon in terms of age, gender and region were analyzed and summarized. It was found that: (1) older patients are more likely to have fixed and acute angulation of sigmoid colon as well as higher contact friction than younger patients due to previous pelvic diseases; (2) females tend to have longer and deeper transverse colons and lower position of sigmoid-descending junctions compared with males; (3) colon diameter is one of the main anatomical differences for the bowel of patients from different regions. These summaries were further used for developing colon models during the simulation stage.

In the stage of insertion simulation, to represent the anatomic difference of patients in terms of age, a rectosigmoid junction (RSJ) model with different contact friction coefficients was developed. To represent the anatomic difference of patients in terms of region, a rectosigmoid junction (RSJ) model with two different colon diameters was developed. To represent gender induced anatomic difference of patients, a rectum-

splenic flexure segment (RSF) model with angle α=0°, 30° and 45° and a transverse-hepatic flexure segment (THF) model with angle β= 0°, 30° and 45° were developed. The colonoscope was modeled as a slender cylinder with a hemisphere tip and 3 different shaft diameters were used (12.8mm SDC, 11.3mm PDC and 9.2mm UTC). The colon tissue was modeled as an isotropic homogenous 3 parameters mooney-rivlin hyperelastic material, and the colonoscope was modeled as an elastic material.

Colon deformation during the insertion simulation within each colon model was investigated and compared. The results showed that, compared with the SDC: (1) a SC colonoscope (an UTC or an PDC) caused less colon deformation when negotiating the fixed rectosigmoid junction and was less sensitive to the increase of contact friction; (2) a SC colonoscope showed more reduction of colon deformation for the RSJ model with smaller internal diameter derived from European patients compared with African patients; (3) SC colonoscopes produced less colon deformation for RSF and THF model with the angle α, β= 45°. However, it didn't show any obvious reduction of colon deformation for RSF model with α = 30°, and PDC even caused more colon deformation for THF model with β= 30°. As for RSF and THF models with α, β= 30°, it was noticed that SC colonoscopes caused slightly more colon deformation. In addition, an insertion simulation of the colonoscope within the fixed THF model was conducted to investigate the buckling behavior of the colonoscope and the contact force. Simulation results showed that SC colonoscopes buckled more easily and quickly than SDC, but the contact force between buckled SC colonoscopes were less than that of SDC and the differences in magnitude showed positive correlations with the angle β. Such a result may explain why

SC colonoscopes caused less colon deformation for RSF and THF models with larger angles α and β , respectively, even if they have easier buckling shafts.

Based on corresponding simulation results, the influence of patient characteristics, including age, region and gender on the efficacy of SC colonoscopes in terms of reducing patient pain could be further predicted. Therefore, the following conclusions could be achieved, 33i.e, SC colonoscopes are more efficient in reducing patient pain for older patients, patients with smaller colon diameters and female patients.

Such a numerical model developed in this thesis serves as the starting point in understanding the effects of age, region and gender of patients on the performance efficiency of SC colonoscopes in terms of reducing patient pain.

6.2 Future Work

The main limitations of this study are the followings: (1) we did not consider the anisotropic properties of colon tissue. Since the mechanical stretch of the colonic wall induced by a colonoscope is mainly along longitudinal direction, an isotropic, incompressible hyperelastic model was selected to model the tensile properties of colon tissue in our work. An anisotropic fiber-reinforced hyperelastic model would have led to more accurate characterizations of colonic tissue properties and could be applied in our future work. (2) we did not consider the influence of age, region and gender on the material properties of the human colon. To include such influence in our model may lead to more accurate simulation results. Therefore, studying the differences of the material properties of the human colon with respect to age, gender and region will be one of my future work. (3) the model of a colonoscope did not include an active bending section. The angulation of active bending is controlled by endoscopist through control knobs and

cables and thus it couldn't be simulated in our model. However, the endoscopists' skill has large influence on maneuvering the bending section. Excluding such bending section may also eliminate the disturbance of endoscopists' experience existing in RCTs. (4) the validation process by designing corresponding experiment was lacked in our work. Since it is very difficult to measure the deformation of the colon through experiment, investigate contact force and distal end displacement of the colonoscope may be better choice based on idea from the insertion simulation in fixed THF model.

REFERENCE

A. Duménil, A. Kaladji, M. Castro, S. Esneault, A. Lucas, M. Rochette, C. Goksu and P. Haigron, "Finite-Element-Based Matching of Pre- and Intraoperative Data for ImageGuided Endovascular Aneurysm Repair," IEEE Transactions on Biomedical Engineering, vol. 60, no. 5, pp. 1353-1362, 2013.

Abaqus. 2011. Abaqus Theory Manual (v.6.11). Dassault Systèmes.

Advanced Analysis Techniques Guide, ANSYS 2009, Inc.

American Accreditation HealthCare Commission. http://www.urac.org.

Balaguru, D., Bhalala, U., Haghighi, M., & Norton, K. (2011). Computed tomography scan measurement of abdominal wall thickness for application of near-infrared spectroscopy probes to monitor regional oxygen saturation index of gastrointestinal and renal circulations in children. Pediatric Critical Care Medicine, 12(3). DOI: 10.1097/PCC.0b013e3181e8b430

Bathe, K. J., Finite Element Procedures, Prentice-Hall, Englewood Cliffs, NJ. 1982

Blausen.com staff. "Blausen gallery 2014". Wikiversity Journal of Medicine 1 (2). doi:10.15347/wjm/2014.010. ISSN 200187

Brenner H, Chang-Claude J, Jansen L et al (2014) Reduced risk of colorectal cancer up to 10 years after screening, surveillance, or diagnostic colonoscopy. Gastroenterology 146:709–717

Carniel, E. L., et al. (2014). "Characterization of the anisotropic mechanical behaviour of colonic tissues: experimental activity and constitutive formulation." Experimental Physiology **99**(5): 759-771.

Carniel, E. L., et al. (2014). "Constitutive formulations for the mechanical investigation of colonic tissues." J Biomed Mater Res A **102**(5): 1243-1254.

Chen PJ, Shih YL, Chu HC et al. A prospective trial of variable stiffness colonoscopes with different tip diameters in unsedated patients. Am J Gastroenterol 2008; 103: 1365–1371

Chen PJ, Shih YL, Chu HC, Chang WK, Hsieh TY, Chao YC. A prospective trial of variable stiffness colonoscopes with different tip diameters in unsedated patients. Am. J. Gastroenterol. 2008; 103: 1365–71.

Chen PJ, Shih YL, Chu HC, Chang WK, Hsieh TY, Chao YC. A prospective trial of variable stiffness colonoscopes with different tip diameters in unsedated patients. *Am. J. Gastroenterol.* 2008; 103: 1365–71.

Chen, YK & Powis, ME. The structure and function of the video image endoscope. In: Gastrointestinal disease: an endoscopic approach, 2nd edn, 2002 pp. 16–23

Cheng, W. B., et al. (2012). "Analysis of and mathematical model insight into loop formation in colonoscopy." Proceedings of the Institution of Mechanical Engineers Part H-Journal of Engineering in Medicine **226**(H11): 858-867.

Choi, J., & Drozek, D. (2012). Analysis of the Looping Problems in Colonoscopy Using Bending Sensors. Journal of Medical Devices, 6(1), 017554.

Christensen, M., Oberg, B., & Wolchok, K. (2015). Tensile properties of the rectal and sigmoid colon: A comparative analysis of human and porcine tissue. SpringerPlus, 4(1), 1-10.

Church JM. Complete colonoscopy: How often. And if not, why not. Am J Gastroenterol,1994;89:556-560

Cook, R. D., Malkus, D.S., and Plesha, M.E., Concepts and Applications of Finite Element Analysis, Second Edition, John Wiley and Sons, New York (1981).

Egorov, Schastlivtsev, Prut, Baranov, & Turusov. (2002). Mechanical properties of the human gastrointestinal tract. Journal of Biomechanics, 35(10), 1417-1425.

Fagan, J, Finite Element Analysis: Theory and Practice, 1992, Longman Scientific & Technical: Essex.

Farraye FA, Horton K, Hersey H. Screening flexible sigmoidoscopy using an upper endoscope is better tolerated by women. Am J Gastroenterol 2004; 99: 1074–1080

Ferlay J, Soerjomataram I, Ervik M et al (2013) GLOBOCAN 2012 v1.0, Cancer Incidence and Mortality Worldwide: IARC CancerBase No. 11. International Agency for Research on Cancer: Lyon, France. 2013

Ferlay J, Soerjomataram I, Ervik M et al (2013) GLOBOCAN 2012 v1.0, Cancer Incidence and Mortality Worldwide: IARC CancerBase No. 11. International Agency for Research on Cancer: Lyon, France. 2013

Ferlay J, Soerjomataram I, Ervik M et al (2013) GLOBOCAN 2012 v1.0, Cancer Incidence and Mortality Worldwide: IARC CancerBase No. 11. International Agency for Research on Cancer: Lyon, France. 2013

Gabella G (1987). The cross-ply arrangement of collagen fibres in the submucosa of the mammalian small intestine. Cell Tissue Res 248, 491–497.

Gao, D., & Huang, W. (2015). A review of down-hole tubular string buckling in well engineering. Petroleum Science, 12(3), 443-457.

Garborg KK, Loberg M, Matre J, Holme O, Kalager M, Hoff G, Bretthauer M (2012) Reduced pain during screening colonoscopy with an ultrathin colonoscope: a randomized controlled trial. Endoscopy 44:740–746

Hajianmaleki, & Daily. (2014). Advances in critical buckling load assessment for tubulars inside wellbores. Journal of Petroleum Science and Engineering, 116, 136-144.

Han Y, Uno Y, Munakata A. Does flexible small-diameter colonoscope reduce insertion pain during colonoscopy? World J Gastroenterol 2000; 6: 659–663

Hidovi´c-Rowe D & Claridge E (2005). Modelling and validation of spectral reflectance for the colon. PhysMed Biol 50, 1071–1093.

Hokeš, F., Kala, J., Krňávek, O., Nonlinear Numerical Simulation of a Fracture Test with Use of Optimization for Identification of Material Parameters, International Journal of Mechanics, 10 (2016) 159-166.

Hsieh, Y. H., Tseng, C. W., Koo, M. T., Hu, C., & Leung, F. (2017). Prospective multicenter randomized controlled trial comparing adenoma detection rate in colonoscopy using water exchange, water immersion, and air insufflation. Gastrointestinal Endoscopy, 86(1), 192-201.

Huang, Gao, & Wei. (2015). Local mechanical model of down-hole tubular strings constrained in curved wellbores. Journal of Petroleum Science and Engineering, 129, 233-242.

HuangZ, ZhengW, XieS, ChenR, ZengH, McLeanDI&Lui H (2004). Laser-induced autofluorescence microscopy of normal and tumor human colonic tissue. Int J Oncol 24, 59–63.

ICRU, 1992b. Photon, Electron, Proton and Neutron Interaction Data for Body Tissues. ICRU Report 46. International Commission on Radiation Units and Measurements, Bethesda, MD

J. Gindre, A. Bel-Brunon, A. Kaladji, A. Duménil, M. Rochette, A. Lucas, P. Haigron and A. Combescure, "Finite element simulation of the insertion of guidewires during an EVAR procedure; example of a complex patient case, a first step toward patient-specific parameterized models," International Journal for Numerical Methods in Biomedical Engineering, vol. 7, no. 31, 2015.

J.A. Weiss, J.C. Gardiner and C. Bonifasi-Lista, Ligament material behavior is nonlinear, viscoelastic and rate independent under shear loading, J. Biomech. 35 (2002), 943–950.

Jia, Hui, Pan, Yanglin, Guo, Xuegang, Zhao, Lina, Wang, Xiangping, Zhang, Linhui, . . . Fan, Daiming. (2017). Water Exchange Method Significantly Improves Adenoma Detection Rate: A Multicenter, Randomized Controlled Trial. The American Journal of Gastroenterology, 112(4), 568-576.

Junqueira LC, Carneiro J & Long JA (2005). Basic Histology, 11th edn. McGraw-Hill Medical Publishing, New York.

Kalaji, A. Dumenil, M. Castro, A. Cardon, J.-P. Becquemin, B.-S. Benyebka, A. Lucas and P. Haigron, "Prediction of deformations during endovascular aortic aneurysm repair using finite element simulaiton," Computerized Medical Imaging and Graphics, no. 37, pp. 142-149, 2013.

Keswani, R. (2012). Successful Colonoscopy in Patients Referred for Prior Incomplete Colonoscopy Does Not Require More Time but Often Requires Use of a Different Endoscope. Gastrointestinal Endoscopy, 75(4), 355.

Kim WH, Cho YJ, Park JY, Min PK, Kang JK, Park IS (2000) Factors affecting insertion time and patient discomfort during colonoscopy. Gastrointest Endosc 52:600–605

Kim, Sy, Chung, JW, Park, Dk, Kwon, Ka, Kim, Ko, Kim, Yj, & Kim, Jh. (2017). Comparison of carbon dioxide and air insufflation during consecutive EGD and colonoscopy in moderate-sedation patients: A prospective, double-blind, randomized controlled trial. Gastrointestinal Endoscopy, 85(6), 1255-1262.

Kozarek RA, Botoman VA, Patterson DJ. Prospective evaluation of a small caliber upper endoscope for colonoscopy after unsuccessful standard examination. Gastrointest. Endosc. 1989; 35: 333–5.

Kunath, S., et al. (2015). Effective Parameter Identification to Validate Numerical Simulation Models.

Lehký, D., Novák, D., Inverse reliability problem solved by artificial neural networks, In: Safety, Reliability, Risk and Life-Cycle Performance of Structures and Infrastructures, New York, USA, (2013) 5303-5310.

Loeve, A., Fockens, P., & Breedveld, A. (2013). Mechanical analysis of insertion problems and pain during colonoscopy: Why highly skill-dependent colonoscopy routines are necessary in the first place ... and how they may be avoided. Canadian Journal of Gastroenterology, 27(5), 293-302.

LS-DYNA. 2013 Theoretical Manual (R 7.0). Livermore Software Technology Corporation

Luo DJ, Hui AJ, Yan KK, Ng SC, Wong VW, Chan FK, Cheong JP, Lam PP, Tse YK, Lau JY (2012) A randomized comparison of ultrathin and standard colonoscope in cecal intubation rate and patient tolerance. Gastrointest Endosc 75:484–490

Manser CN, Bachmann LM, Brunner J et al (2012) Colonoscopy screening markedly reduces the occurrence of colon carcinomas and carcinoma-related death: a closed cohort study. Gastrointest Endosc 76:110–117

Manser CN, Bachmann LM, Brunner J et al (2012) Colonoscopy screening markedly reduces the occurrence of colon carcinomas and carcinoma-related death: a closed cohort study. Gastrointest Endosc 76:110–117

Marshall JB, Perez RA, Madsen RW. Usefulness of a pediatric colonoscope for routine colonoscopy in women who have undergone hysterectomy. Gastrointest Endosc 2002; 55: 838–841

Massalou, Masson, Foti, Afquir, Baqué, Berdah, & Bège. (2016). Dynamic biomechanical characterization of colon tissue according to anatomical factors. Journal of Biomechanics, 49(16), 3861-3867.

Mitchell, R., McCallion, K., Gardiner, K., Watson, R., & Collins, J. (2002). Successful colonoscopy; completion rates and reasons for incompletion. The Ulster Medical Journal, 71(1), 34-37.

Most, T., Identification of the parameters of complex constitutive models: Least squares minimization vs. Bayesian updating, Reliability Conference in München, (2010).

Nemoto, D., Utano, K., Endo, S., Isohata, N., Hewett, D., & Togashi, K. (2017). Ultrathin versus pediatric instruments for colonoscopy in older female patients: A randomized trial. Digestive Endoscopy, 29(2), 168-174.

Ní Ghriallais, R. and M. Bruzzi (2014). "A Computational Analysis of the Deformation of the Femoropopliteal Artery With Stenting." Journal of Biomechanical Engineering **136**(7): 071003-071003-071010.

Nivatvougs S, Fryd DS, Fang D. How difficult is colonoscopy? (Abstract). Gastrointest Endosc, 1982;28:140

Ogawa, T., Ohda, Y., Nagase, K., Kono, T., Tozawa, K., Tomita, T., . . . Miwa, H. (2015). Evaluation of discomfort during colonoscopy with conventional and ultrathin colonoscopes in ulcerative colitis patients. Digestive Endoscopy, 27(1), 99-105.

optiSLang, Methods for multi-disciplinary optimization and robustness analysis, Dynardo GmbH, Weimar, Germany, (2014).

Park CH, Lee WS, Joo YE et al. Sedation-free colonoscopy using an upper endoscope is tolerable and effective in patients with low body mass index: a prospective randomized study. Am. J. Gastroenterol. 2006; 101: 2504–10.

ParkCH, LeeWS, JooYEetal. Sedation-free colonoscopy using an upper endoscope is tolerable and effective in patients with low body mass index: a prospective randomized study. Am J Gastroenterol 2006; 101: 2504–2510

Pasternak, Artur, Szura, Miroslaw, Solecki, Rafal, Matyja, Maciej, Szczepanik, Antoni, & Matyja, Andrzej. (2017). Impact of responsive insertion technology (RIT) on reducing discomfort during colonoscopy: Randomized clinical trial. Surgical Endoscopy, 31(5), 2247.

Petr Král, Petr Hradil, & Jiří Kala. (2017). Inverse identification of the material parameters of a nonlinear concrete constitutive model based on the triaxial compression strength testing. Frattura Ed Integrità Strutturale, 11(39), 38-46.

Rajagopalan, R., Deodurg, P., & Srikanth. (2013). Overview of randomized controlled trials. Asian Journal of Pharmaceutical and Clinical Research, 6(3), 32-38.

Ravi J, Brodmerkel GJ Jr, Agrawal RM, Gregory DH, Ashok PS. Does prior abdominal or pelvic surgery affect the length of insertion of the colonoscope (Abstract) Endoscopy, 1988;20:43

Rex DK, Bond JH, Winawer S, Levin TR, Burt RW, Johnson DA, Kirk LM, Litlin S, Lieberman DA, Waye JD, Church J, Marshall JB, Riddell RH (2002) Quality in the technical performance of colonoscopy and the continuous quality improvement process for colonoscopy: recommendations of the U.S. Multi-Society Task Force on colorectal cancer. Am J Gastroenterol 97:1296–1308

Rex DK. Achieving cecal intubation in the very difficult colon. Gastrointest. Endosc. 2008; 67: 938–44.

Ribarren, Carlos; Darbinian, Jeanne A.; Lo, Joan C.; Fireman, Bruce H.; Go, Alan S. (2006). "Value of the Sagittal Abdominal Diameter in Coronary Heart Disease Risk Assessment: Cohort Study in a Large, Multiethnic Population". American Journal of Epidemiology. 164 (12): 1150–9. doi:10.1093/aje/kwj341

Rowland, R., Bell, S., Dogramadzi, G., & Allen, D. (1999). Colonoscopy aided by magnetic 3D imaging: Is the technique sufficiently sensitive to detect differences between men and women? Medical & Biological Engineering & Computing, 37(6), 673-679.

Rust, W. and Schweizerhof, K. (2003) 'Finite element limit load analysis of thin-walled structures by ANSYS (implicit), LS-DYNA (explicit) and in combination', Thin-Walled Structures, Vol. 41, pp.227–244.

Saifuddin T, Trivedi M, King PD, Madsen R, Marshall JB. Usefulness of a pediatric colonoscope for colonoscopy in adults. Gastrointest. Endosc. 2000; 51: 314–7.

Sato K, Shigiyama F, Ito S, Kitagawa T, Tominaga K, Suzuki T, Maetani I (2013) Colonoscopy using a small-caliber colonoscope with passive-bending after incomplete colonoscopy due to sharp angulation or pain. Surg Endosc 27:4171–4176

Saunders, Fukumoto, Halligan, Jobling, Moussa, Bartram, & Williams. (1996). Why is colonoscopy more difficult in women? Gastrointestinal Endoscopy, 43(2), 124-126.

Schmidt CM, Schultz SM, Lee JG, Baillie J. The association between gender and difficult colonoscopy (Abstract). Gastrointest Endosc, 1994;40:46

Streett, S. (2007). Endoscopic colorectal cancer screening in women: Can we do better? Gastrointestinal Endoscopy, 65(7), 1047-1049.

Todd N Witte, & Robert Enns. (2007). The Difficult Colonoscopy. Canadian Journal of Gastroenterology, 21(8), 487-490.

Tox U, Schumacher B, Toermer T, Terheggen G, Mertens J, Holzapfel B, Lehmacher W, Goeser T, Neuhaus H (2013) Propofol sedation for colonoscopy with a new ultrathin or a standard endoscope: a prospective randomized controlled study. Endoscopy 45:439–444

Van Dam, Eickhoff, Jakobs, Kudis, Hartmann, & Riemann. (2006). Computer-Assisted Colonoscopy (the NeoGuide System): Results of the First Human Clinical Trial. Gastrointestinal Endoscopy, 63(5), AB100.

Watters, D., Smith, A., Eastwood, M., Anderson, K., Elton, R., & Mugerwa, J. (1985). Mechanical properties of the colon: Comparison of the features of the African and European colon in vitro. Gut, 26(4), 384-92.

Watters, D., Smith, A., Eastwood, M., Anderson, K., Elton, R., & Mugerwa, J. (1985). Mechanical properties of the colon: Comparison of the features of the African and European colon in vitro. Gut, 26(4), 384-92.

Waye, & Bashkoff. (1991). Total colonoscopy: Is it always possible? Gastrointestinal Endoscopy, 37(2), 152-154.

Wehrmann T, Lechowicz I, Martchenko K, Riphaus A. Routine colonoscopy with a standard gastroscope. A randomized comparative trial in a western population. Int. J. Colorectal Dis. 2008; 23: 443–6.

Welch, C.R., Reid, J.D. Looping Formation During Colonoscopy – a Simulation. 14th International LS-Dyna Users Conference. June 2016

Wex C, Arndt S, Stoll A, Bruns C, Kupriyanova Y. Isotropic incompressible hyperelastic models for modelling the mechanical behaviour of biological tissues: a review. Biomed Tech (Berl). 2015

Whitmer, Lawrence M. Clinical Anatomy of the Large Intestine. Centers for Osteopathic Research & Education. Jan 23, 2007.

Z.W. Wang and C.Y. Tang, Comments on viscoelastic studies of human subscapularis tendon: relaxation test and a Wiechert model, Comput. Meth. Prog. Bio. 96 (2009), 234–235.

Zienkiewicz, O. C., The Finite Element Method, McGraw-Hill Company, London, (1977).